University of Tartu
Institute of Geology

Kristjan Urtson

Melt segregation and accumulation: analogue and numerical modelling approach

MSc. Thesis

Supervisors: PhD Alvar Soesoo
PhD Kalle Kirsimäe

Tartu 2005

CONTENTS

Abstract

Partial melting process and its dynamics was studied on the ground of the observed fractality in migmatite structures and possible self-organized critical nature of magma generation. In the two investigated migmatite outcrops and six drill cores the leucosome thicknesses follow the power law with exponents D=0.83-1.41. In the experiment with sand and carbon dioxide as analogues of the host rock and melt phase, the stepwise transport and accumulation of gas led to the power law distribution of gas batch sizes with an exponent D=0.5. The recalculation of leucosome width and gas batch area distributions to respective volume distributions suggests that melt accumulation into larger leucosomes is not favoured in migmatites, whereas the accumulation of the gas is effective in the analogue experiment. Better accumulation in the experiment is evidently the result of relatively higher mobility of gas compared to the melt in migmatites, as the mobility is the main factor, which enhances the accumulation. Poor accumulation can reflect also poor melt extraction from the migmatite. Little melt is probably extracted from measured migmatites or alternatively, the observed structures result from the last stage melting processes with low melt mobility prior to freezing of migmatite.

Kokkuvõte

Magma segregeerumine ja akumulatsioon: analoog- ja numbriline modelleerimine

Maakoore osalise ülessulamise dünaamikat uuriti lähtudes migmatiitide fraktaalsusest ja iseorganiseeruva kriitilise seisundi võimalikust esinemisest magma moodustumise protsessides. Kahes migmatiidipaljandis ja kuues puuraugus mõõdetud leukosoomide paksused järgivad astmejaotusi eksponentidega D=0.83-1.41. Eksperiment liiva ja süsihappegaasiga kui algkivimi ja magma analoogidega tõendab, et gaasi astmelise transpordi ja akumulatsiooni tulemuseks on gaasikogumite suuruste astmejaotus, antud juhul eksponendiga D=0.5. Leukosoomide paksuste jaotuste ja gaasikogumite pindalade jaotuse ümberarvutus vastavateks ruumalade jaotusteks näitab, et mõõdetud migmatiitides ei ole magma kogunemine suurematesse leukosoomidesse olnud soodustatud, samas kui analoogeksperimendis on gaasi akumulatsioon efektiivne. Ilmselt on akumulatsioon eksperimendis parem tänu gaasi suuremale mobiilsusele võrreldes magmaga, kuna mobiilsus on määrav tegur akumulatsiooni efektiivsusel. Ebaefektiivne akumulatsioon võib peegeldada ka ebaefektiivset magma lahkumist, seega võib uuritud migmatiitidest olla vähe magmat lahkunud või alternatiivselt, nähtav migmatiitide struktuur on tekkinud magma vähese mobiilsuse tõttu vahetult enne migmatiidi lõplikku hangumist.

1. INTRODUCTION

Partial melting and the melt extraction from its source rock is the main mechanism of magma generation in the Earth's crust. Starting on micrometre-scale at the grain contacts, the produced melt will segregate, accumulate and ascend to the upper part of the crust, where it forms large magma bodies in volumes of kilometre-scale. The whole range of magma formation and accumulation processes thus covers up to ten orders of magnitude. However, the mechanisms how the melt is transported from grain-scale to the plutons, are still poorly understood.

Migmatites are one of the manifestations of partial melting in the crust. The picture one can see in migmatites represents a frozen moment of magma generation processes, that have once taken place in a crustal segment at the deeper level, and which is now exposed on the surface as a migmatized rock. Apparently, the migmatization has been interrupted at some stage in-between, leaving the structure of migmatite in the form it has acquired as the result of melt segregation, accumulation and transport.

As the traces of previous processes are rare, only the end product of the magma generation prior to freezing is observable in migmatites. There is little evidence about the melting stage, where the system has been solidified, or about magma volume, that has been produced and extracted from the migmatite under observation, or about processes that have been involved. Although geochemical methods can be used to estimate possible generated melt volumes, they cannot say much about process dynamics.

Emerging fractality in migmatites suggests possible self-organized critical and scale invariant behaviour of magmatic systems as the originator of fractal structures. The scale invariant nature of magma generation and transport processes allows to assume their probable similarity over the whole range of orders of magnitude, forming a continuum from micrometre- to kilometre-scale.

This work, however, deals with features at the lower end of that range, up to the outcrop scale. The purpose of this work is to show that the investigation of the dynamics of partial melting processes, that are responsible for generating the fractality observed in migmatites is principally possible by using analogue and numerical methods and that information about the formation of migmatites can be inferred from their fractal nature.

In subsequent chapters, some insight will be given into current theories of magma formation and migration, as well as into the nature of fractals and self-organized criticality as essential constituents of the proposed approach.

As the groundwork of all consecutive interpretations on the origin of migmatite structure, the results of leucosome width measurements in migmatites will be presented. Leucosome thicknesses have been measured in six drill cores from Estonian crystalline basement and in outcrops of Masku, southwestern Finland and Montemor-o-Novo, central Portugal, suggesting the possible scale invariance of partial melting processes.

An experiment using analogue materials was carried out, offering a possibility to directly observe processes of liquid phase accumulation and transport in solid granular matrix. The experiment allows to draw parallels to processes, that can be involved in partial melting of the crust.

On the ground of this experiment, the formation of fractal structures in migmatites is discussed in the context of a numerical simulation of melt accumulation and transport processes.

2. MIGMATITES AND MAGMA TRANSPORT

2.1 Migmatization

Migmatization is considered to take place when metamorphic conditions (temperature and pressure) are suitable to melt the crustal material and produce magma. This can happen in the lower part of the crust, where temperature at the typical geothermal gradient (20ºC/km) is high enough to induce on the presence of the water the melting of the rock. This, however, can produce only a limited amount of magma up to 25% of the rock volume. Melting of higher volumes of the crust in dry (fluid-deficient) conditions requires an extra heating, which can be attained by heat conduction from nearby magma bodies, e.g. by underplating of hot mafic magmas derived from the mantle (Petford et al., 2000).

The production of magma continues until the temperature finally decreases due to the uplift of the crustal block or weakening of the thermal event. The migmatization process will be interrupted and the system freezes in the reached state. Further uplift and following erosion can expose the migmatized crustal segment, so one can on the surface directly observe a frozen moment from migmatite formation process.

Migmatite is a macroscopically composite rock, which consists of leucocratic and melanocratic parts. The leucocratic part is of magmatic appearance and has evidence of higher mobility (Kriegsman, 2001), whereas the melanocratic part is metamorphosed country rock in general term.

Commonly leucocratic and melanocratic domains form characteristic migmatitic banding, such type of migmatite is called metatexite or stromatic migmatite. If the migmatitic banding is absent or disrupted due to the high melt content, the rock is called diatexite (Kriegsman, 2001).

Various models have been proposed in the last hundred years to explain the origin of the banded structure of migmatites (Maaløe, 1992; Mengel et al., 2001):

- injection of foreign magmas along foliation planes
- anatexis (partial melting) and melt segregation
- concentration of water along foliation as melting initiator
- heterogeneous character of the protolith prior to migmatization
- metasomatism
- metamorphic differentiation

• combination of anatexis and metasomatism.

However, in recent years partial melting along with the melt segregation is considered to be the dominant process of migmatite formation (Mengel et al., 2001). The consensus today is that both *in situ* melt and externally derived melt are present in most migmatites (Kriegsman, 2001).

2.2 Migmatite structure

Petrologically three different structural elements can be distinguished in migmatites (Figure 1):

- leucosome, which has an igneous origin and consists mainly of felsic components (Johannes et al., 2003)
- mesosome, which consists of felsic and mafic minerals, has usually composition of bulk migmatite and is referred to as protolith or parent rock (Maaløe, 1992)
- melanosome— thin layer of dark minerals, which separates leucosome from the mesosome, although not invariably (Kriegsman, 2001).

The opinions about the origin of these domains are contradictory. Leucosome and melanosome together are often called a neosome and mesosome in this context a paleosome as unaltered parent rock. The melanosome is considered to be restite where refractory minerals become concentrated when mobile minerals are transferred into leucosome. The melt is thus originated from the melanosome, whereas the composition of the mesosome has been remained unaffected (Maaløe, 1992). On the contrary, many authors (e.g. Kriegsman, 2001) suggest that mesosome has undergone significant melt extraction, is therefore restitic and does not represent the composition of the protolith. The melanosome is formed either by the retrograde back reactions of melt with the mesosome or by the crystallizing and accumulation of mafic minerals from the melt in leucosomes. The truth may be the combination of all the above-mentioned models (Kriegsman, 2001).

Questionable is also the origin of leucosome as the equivalent of crystallized melt. Some leucosomes may represent either cumulates, formed by fractional crystallization from primary granitic melt (Johannes et al., 2003) or their composition can be affected by the back reaction between the restite and crystallizing melt (Kriegsman, 2001).

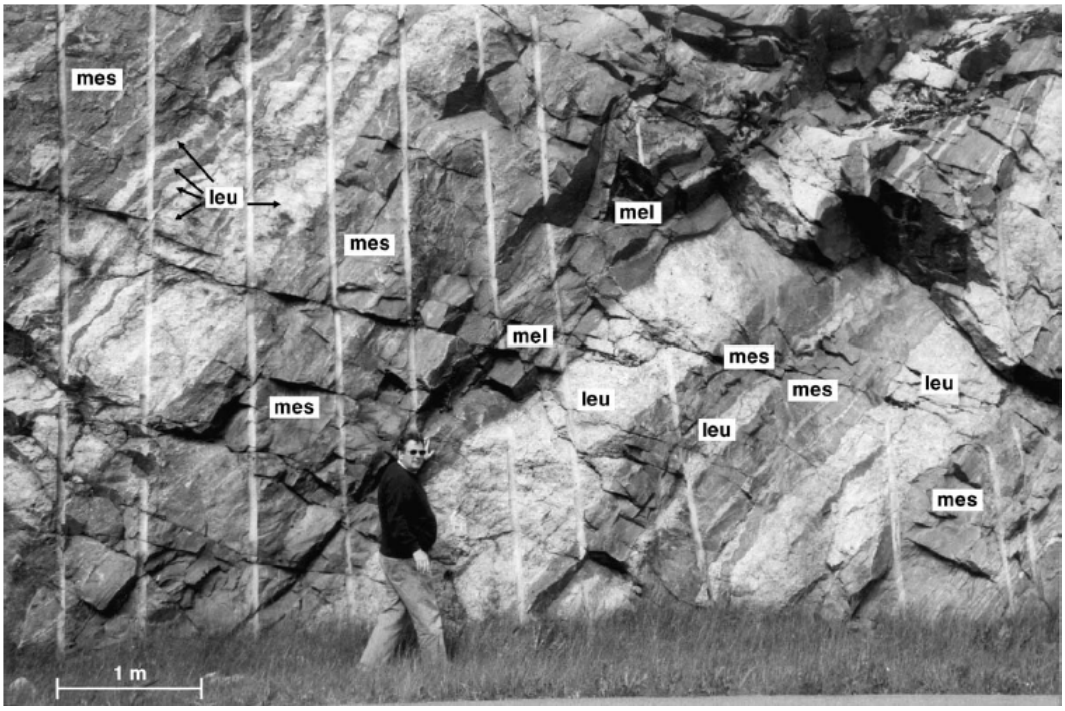

Figure 1. Photograph of a road cut in Turku area, Finland, displaying structural relationships between leucosomes (leu), melanosomes (mel) and mesosomes (mes) (Johannes et al., 2003).

Mengel et al. (2001) distinguished three different types of leucosomes as a result of various degrees of melt segregation and transport: 1) *in situ* leucosomes, which are centimetre thick patches of melt that formed almost in place and are the result of very limited melt segregation; 2) decimetre to two metre thick coarse-grained leucosome sills, that represent the most mobile melt fraction, which is considered to have migrated tens of metres; 3) centimetre-to decimetre thick composite leucosomes where the melt has been transported over relatively short distances (< 1 m). The latter type is associated with the restite-rich melanosomes and is considered as a link between *in situ* leucosomes and leucosome sills.

In addition to layer-parallel leucosomes, commonly centimetre to metre wide discordant dykes are present in migmatites, that cross-cut the migmatitic banding (Maaløe, 1992; Marchildon & Brown, 2003). Many of these dykes are structurally and compositionally closely related to the adjacent leucosomes and are thus simultaneous, which indicates high mobility of the melt during crustal anatexis.

2.3 Melting processes, magma segregation and transport

Migmatites are therefore the result of the different processes in combination- partial melting, melt segregation, extraction and magma transport.

The melting of the crustal rock starts at the microscopical scale at grain contacts, preferentially between feldspar and quartz crystals (Knesel & Davidson, 1999). The initial melt will reside at three or four grain junctions in tiny isolated melt pockets, which geometry is controlled by wetting angle (i.e. surface energy differences) between solid and liquid phases (Walte et al., 2003, Figure 2). Magma is formed by connecting a large number of such grain-scale domains and draining the melt from the solid fraction, a process called melt segregation (Sawyer, 2001). Increase of melt fraction will cause melt pockets to grow until they get connected to each other by melt film formed on grain surfaces. At this point, a three-dimensional melt framework is created.

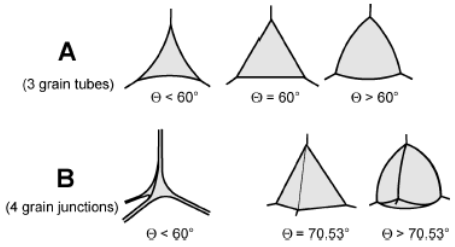

Figure 2. Schematic representation of liquid-phase equilibrium geometry. A: Perpendicular to three-grain tubes. B: Four-grain junctions. Interconnected liquid network forms only at Θ<60˚ (Walte et al., 2003).

The formation of interconnected melt network thus depends on the geometry of melt pockets and partial melting rate. Obviously, the higher wetting angle requires higher melt volume for melt pockets to become interconnected. Based on high-temperature experiments with major rock forming minerals, low values of wetting angle (12 to 60º) between quartz and feldspar crystals and melt have been reported; connectivity threshold of 3-4% melt is predicted for partially molten amphibolite and therefore, low wetting angles should be a general rule during the crustal anatexis (Laporte and Watson, 1995). Vigneresse et al. (1996) suggested a minimum of 8% melt fraction for felsic melts to overcome the liquid percolation threshold and allowing local magma displacement. In this case, the transport of the magma is performed by the flow through pore space, which is controlled by permeability of the rock. However, the interaction of melt with cooler ambient rock sets the limit to the distance of magma transport and the flow through pores can thus not account for transfer of significant melt volumes.

Another threshold of 15-20% of melt volume is needed to break the cohesion between mineral grains, which allows the melt to escape from the local system and the magma transfer over large distances. This marks the transition from the closed system to an open one (Vigneresse et al., 1996). On the other hand, Bons et al. (2004) argued, that neither connected melt network, nor reaching any threshold is required to accomplish magma segregation. According to their conceptual model, magma is transported discontinuously in the melt batches and the accumulation occurs by the stepwise merging of the batches. As a result, magma transport and extraction can take place at very low melt fractions.

The melt transport in accordance with the model of Bons et al. (2004) is possible, when melt fraction in partially molten rock is inhomogeneously distributed or stress field applied is heterogeneous (and probably they are). The bulk melt fraction in the rock can be low, but in local portions high enough to overcome the liquid percolation and melt escape thresholds, so a batch of melt becomes mobile. While migrating toward the nearby site with the low melt content, the melt fraction there will increase, causing the melt to overcome the threshold, become mobile and so on. This is consistent with the numerical model of Vigneresse & Burg (2000): as long as melt content remains low, the segregation cannot achieve sufficient production and is rather discontinuous; although at higher melt fraction, it is continuously extracted.

As a driving force, deformation of the rock plays a major role in magma segregation. The movement of the melt is controlled by pressure gradients, i.e. melt tends to migrate toward sites where the pressure is lower. Deformation strongly enhances melt segregation as tectonic stress gradients can be up to two orders of magnitude higher than gradients created by buoyancy forces. Nevertheless, as the size of a melt batch increases, buoyancy becomes more important for melt mobility (Bons et al., 2004). The melt segregation without deformation is limited due to the high viscosity of the melt, especially that of granitic magma. Therefore deformational forces are needed to squeeze the melt out of the matrix (Vigneresse et al., 1996). Pure shear, i.e. the compaction of the rock is effective on melt concentration, which results in the melt segregation into low stress regions, that are usually oriented to a plane at high angle or perpendicular to major compression (Vigneresse et al., 1996; Vigneresse & Burg, 2000). This is likely the process that may account for leucosome formation. Compaction alone is not sufficiently effective to extract the melt from the rock. Gradients in normal stress field or non-coaxial forces as simple shear component must be added to enhance the mobility of the melt along leucosomes

(Vigneresse & Burg, 2000; Bons et al., 2004). The deformational "pumping" may be assisted by injecting of melt from the adjacent areas.

The increase of volume of about 10% associated with melting can lead to the development of fractures system in the rock providing pathways for melt escape and also create additional gradients in the melt pressure (Vigneresse et al., 1996). However, the existence of the rocks, where melt volume expansion is negative or at very small magnitude, suggests that volume increase by melting cannot be a significant factor in driving the melt segregation (Sawyer, 2001). The fracturing of the rock can appear also as a result of the presence of melt in intergranular spaces as far as the melt pressure, which is close to lithostatic pressure, may reduce effective normal stresses to the point, where failures occur and microfractures form (Bons et al., 2004).

2.4 Estimation of expelled melt volume

The answers to the question of the melt volume produced during migmatization rely mainly upon geochemical data. Melt production is favoured by the presence of the water in the rock. Content of free water in the pore space is usually too low to produce significant amount of magma and the water required is most probably released by the dehydrating of hydrous minerals, such as muscovite and biotite, at higher temperatures (Mengel et al., 2001). The estimations of produced melt volumes are thus based on the pressure- temperature history of the rock, which controls the dehydration and melting processes, and on the fraction of hydrous minerals. The water amount produced by the breakdown of these minerals is used to calculate the generated melt volumes. The melt fractions of 20-30% estimated by this method are reported in migmatites (Mengel et al., 2001; Johannes et al., 2003).

The main problem of such calculations is the amount of hydrous minerals, that were dehydrated during anatexis. This is derived from the difference between the mineral fractions in the rock, that has undergone partial melting (a measurable parameter) and that of the host rock, which is only supposable. Thus the estimations of the volume of expelled melt during anatexis remain speculative.

Another way to study magma generation on the ground of geochemistry is to use the Rare Earth Element (REE) data by comparing the contents and ratios of lanthanoids in the generated melt and host rock (e.g. Mengel et al., 2001). However, migmatites result in most cases of different processes, such as magma migration, mixing, fractional

crystallisation, back reactions with host rock etc. As a consequence, the geochemical record of the melt can appear too complex for its application in the studies of the dynamics of magma processes and the estimations of the produced melt volumes.

3. FRACTALS AND THEIR USE IN GEOSCIENCES

3.1 Definition of a fractal

Unlike the Euclidean geometry, where objects have integer dimensions, fractals refer to objects, that have a non-integer, or fractional (fractal) dimension. The concept of fractional dimension was originally introduced by Benoit Mandelbrot in 1967. Since then, the concept of fractals has found a wide applicability in a broad range of fields of knowledge.

In order to explain and illustrate the nature of fractal dimension, a geometrical fractal called Sierpinski carpet can be constructed (Turcotte, 1992). At the starting point, there is one square with the sides of a unit length (Figure 3, a). The original square will be divided into nine squares with the sides of 1/3 units and the centre square will be removed (Figure 3, b). The same operation is performed on the remaining squares at the next orders of construction (Figure 3, c-e), resulting in 4096 squares with the side length of 1/81 units at the 5th step. Theoretically, this operation can be repeated infinitely. At any step, the number of squares increases eight times and the side length of a square is one third of the square at the former step. The number of squares as a function of the side length A is expressed mathematically by power law as

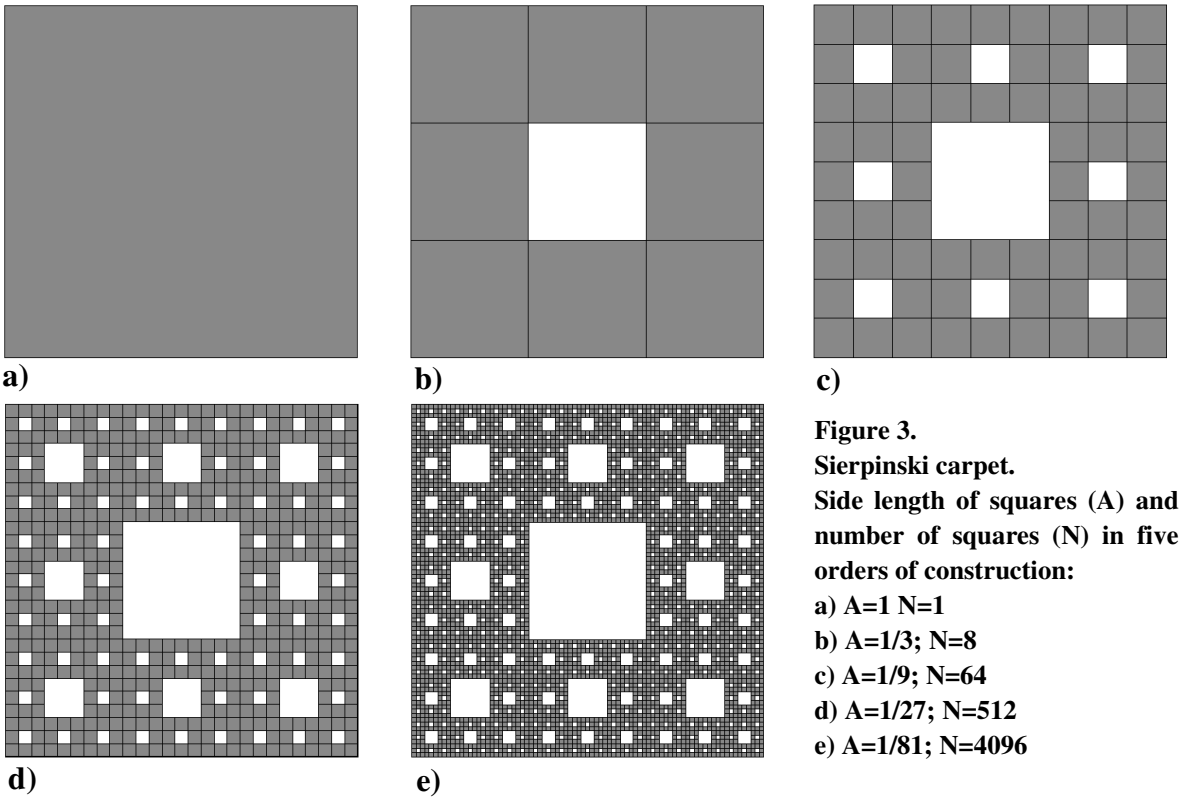

Figure 3.
Sierpinski carpet.
Side length of squares (A) and number of squares (N) in five orders of construction:
a) A=1 N=1
b) A=1/3; N=8
c) A=1/9; N=64
d) A=1/27; N=512
e) A=1/81; N=4096

$$N_A = A^{-D} \quad , \tag{1}$$

where the distribution exponent D is the fractal dimension. The dimension for Sierpinski carpet can be calculated as D=log8/log3=1.8928. If the central squares are not removed, then the dimension would be D = log9/log3 = 2, which is Euclidean dimension of the surface. With its fractal dimension of 1.8928, the Sierpinski carpet lies between the line and the surface. The fractal dimension can be derived also geometrically, when the size of the square and the number of squares bigger than the specified size are plotted on a log-log graph (Figure 4), where according to power law, the data points must define a straight line. The slope of the line refers to the fractal dimension.

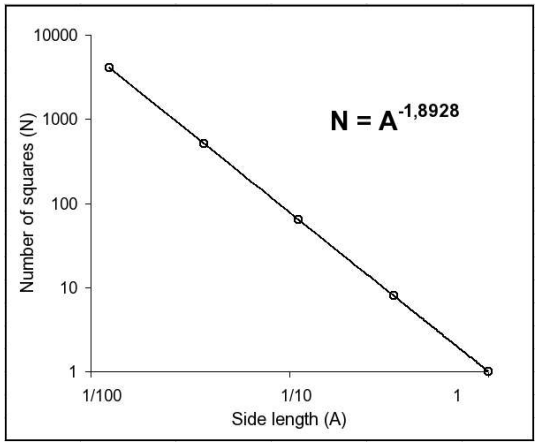

Figure 4.
Side length of a square vs. number of squares greater than that size defining the power law on a log-log plot. The distribution exponent or fractal dimension is 1.8928.

At any step of construction, the Sierpinski carpet consists of eight exact copies of itself, that are reduced three times. This means that Sierpinski carpet is self-similar at any rate of magnification. The self-similarity occurs over many orders of magnitude, which can be infinite as in the case of mathematically constructed fractals, which do not have theoretical limits of maximum and minimum scale. Fractals look the same at any scale and no scale can be preferred. Self-similarity and scale invariance are basic characteristic properties of fractals. One cannot determine the scale of the pattern without a reference- a familiar problem also from (geological) imaging, where a reference object is needed to define the scale (Turcotte, 1992).

In 1967, Mandelbrot introduced his concept of fractional dimension by determining the length of the coast of Britain (Mandelbrot, 1967). The coastline length can be measured on the map covering it with a ruler of certain length. The result, however, depends on the selected ruler resolution, using a shorter ruler allows one to follow finer details on the coastline and thus increases its length. The obtained length as the function of the ruler size

obeys the power law similarly to equation (1) and Figure 4. The power law exponent, or fractal dimension of the west coast of Britain estimated by this method is 1.25 (Bak, 1997), for Norwegian and Estonian coast 1.52 and 1.17, respectively (Engelbrecht & Uus, 1993).

Besides the ruler method, the box counting method can be used to determine the dimension of fractal curves. The number of square boxes needed to cover the curve is counted. The more details on the curve, the more boxes are needed and the higher will be the fractal dimension. The fractal dimension is thus a kind of roughness measure of a curve.

Although deterministic fractals, such as Sierpinski carpet are self-similar over infinite range of scale, naturally occurring fractals have their upper and lower limits. In case of coastline, the upper limit is determined by the size of the island or the continent and the lower limit is set by the smallest ruler, which is meaningful to use. Therefore, in most natural fractals the power law is usually valid only over a few orders of magnitude (Turcotte, 1992).

Self-similar fractal structures are widespread in the nature. The coast consists of fjords and fjords within fjords, large clouds are like enlarged versions of small clouds, mountain ranges include peaks with great variety of height. Fractals are recognized also in river networks, blood vessels, in the structure of the universe as clusters of galaxies, turbulence etc. These are just a few examples. As they are self-similar and scale invariant, no characteristic scale can be specified. There is no typical height of a mountain, no typical size of a cloud or a fjord. There is no “right” size. In the case of, for instance, a Gaussian distribution of objects, a typical measure or mode can be specified.

Geometrical fractals, described above, are fractals in the strict sense. Statistical power law size distributions for the large number of measured objects are also fractal, although in wider meaning. If data follows power law (see Figure 4), the whole range of sizes can be adequately described by the power law exponent. The exponent value determines the mass distribution between the objects- lower exponent flattens the apparent linear trend on the log-log plot, implying the greater significance of larger objects, which contain greater fraction of the mass. Higher value of the exponent, on the other hand, appears on the graph as steeper distribution line, suggesting higher relative importance of small objects and relatively more mass residing in them.

Although statistical power law distribution can be treated as a fractal, the treatment of

the power law exponent as fractal dimension may be somewhat confusing and should be therefore avoided, as the use of dimension is meaningful only for describing spatial structures or spatial distribution of objects (Bonnet et. al., 2001).

Like geometrical fractals, power law distributions are ubiquitous in nature, as well as in fields of human society. Well known is the relationship between earthquake occurring frequency and magnitude, called Gutenberg-Richter law; in biological evolution, the distribution of extinction events follows power law (Bak, 1997). The equation (1) is also called Zipf's law, named after a scientist, who had pointed out the fractal nature of the size distribution of the cities in the world, as well as the frequency of the word use in literature. Similar is also the pattern of unpredictable variations of the stock markets (Bak, 1997).

3.2 The origin of fractals: 1/*f* noise and self-organized criticality

If fractals are spatially or statistically self-similar structures, one-over-*f* noise (also called pink or flicker noise) is a phenomenon, where the self-similarity occurs in time, i.e. it includes fluctuations with durations of all time scales. 1/*f* noise has been observed in very diverse systems as for example, in the radiance of quasars (Figure 5, a), the current through resistors, the sand flow in an hour-glass, the flow of the river Nile and highway traffic (Bak et al., 1987). The signal of 1/*f* noise can be handled as superposition of periodic signals of all frequencies. The strength of a signal component is inversely proportional to its frequency *f*, meaning that the strength is larger for smaller frequencies. The power spectrum of frequencies, that constitute the flicker noise, is a typical power law $S(f)=1/f^{-\beta}$ with exponent β usually roughly equal to 1, although power spectra with exponents between 0 and 2 are also commonly referred to as 1/*f* noise (Bak, 1997). Different from 1/*f* noise is so-called white noise (Figure 5, b), which includes all frequencies in equal amount and which power spectrum is flat. The white noise is comparable with the visible white light, where the components with different wavelengths have equal strength. If the components with longer wavelengths had greater power, the light would appear as pink, that's why 1/*f* noise is often called also a pink noise.

Despite the ubiquity of 1/*f* noise and fractals, their origin is not well understood. Bak et al. (1988) suggested, that some certain complex dynamical systems may independently evolve into a critical state with no characteristic time or length scales. They proposed that such self-organized critical state is the common underlying mechanism behind the both

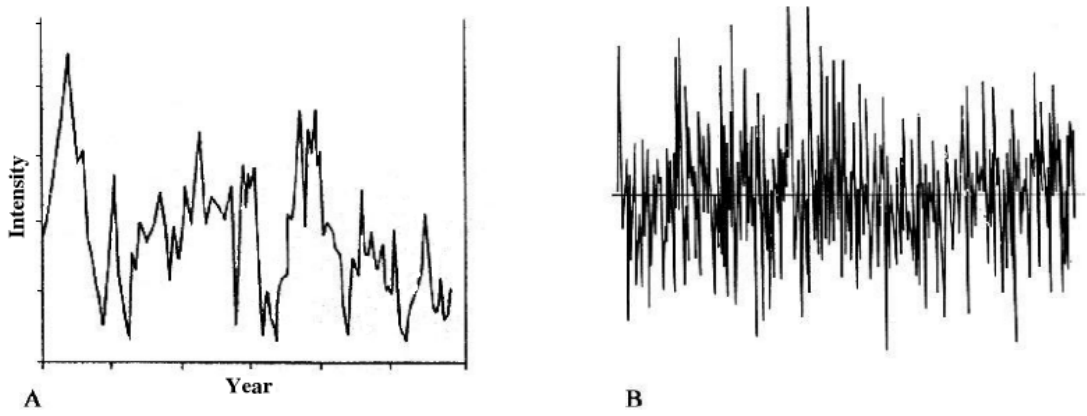

Figure 5. a) Fluctuation of the radiance emitted by a quasar during the period of 80 years- 1/*f* noise; b) white noise (Bak, 1997).

phenomena, 1/*f* noise being it's temporal "fingerprint" and the emergence of fractals corresponding to its spatial signature.

The self-organized criticality occurs then in open complex dynamical systems, with the large number of constituents and far from equilibrium. Complex, spatially and temporally scale-free behaviour occurs only in a narrow range between chaos and order. Also systems in equilibrium, such as phase transitions in mechanics, may exhibit complex behaviour in the critical transition point, but to reach that point, fine tuning of a parameter (e.g. temperature) is needed. Thus, such behaviour may occur only accidentally in the nature. Non-equilibrium critical systems do not need fine tuning of parameters, the self-organization to the critical state is managed by the interaction and interdependence of the system constituents, for example, different species in the ecological system. The critical state is an attractor to the system's dynamics and is always reached independently from the initial conditions (Bak et al, 1987).

In that self-organized critical state, the system is very sensitive to even small external perturbations and responds to them by reorganizing itself. These rearrangements do not take place gradually, but as catastrophes with the sizes of all scales; the catastrophes can be very small or sweep over the entire system. This is where the scale invariant behaviour of a complex system occurs. Due to the cooperation of its constituents, the system always turns back to the critical state with minimal stability (Bak, 1997).

Balancing in the critical state, the system is actually in a punctuated equilibrium with the periods of quiescence, interrupted by the rapid bursts of activity. If the length of quiet periods is comparable with human lifetime, one can conclude, that the system is stable or evolves rather gradually (Bak, 1997).

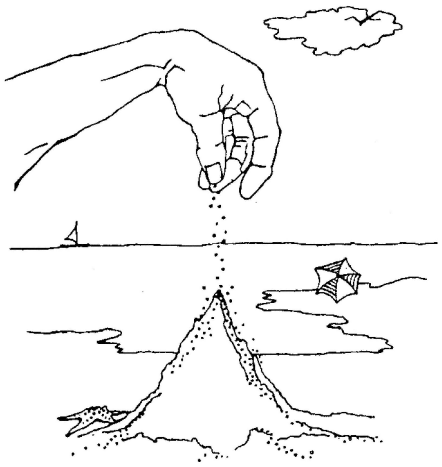

Figure 6. Sand pile system (Bak, 1997).

A classical example of a self-organized critical system is sand pile (Figure 6). Sand is added grain by grain and the slope of the pile slowly increases. In the beginning, when the pile is still flat, grains stay more or less in the place where they land. If the slope reaches a critical value, avalanches occur on the sand pile. A grain that has landed somewhere on the slope, will push its neighbour grain to topple down the slope, which in turn interacts with its neighbours and so on. Such an avalanche may involve the entire pile or terminate after toppling of just few grains. In the critical state, one single grain may cause avalanches with the sizes of all scales. Although the sand pile is somewhat relaxed, or flattened after a catastrophe, the slope builds up again when more sand is added.

In order to apply the theory of self-organized criticality to magma accumulation processes, transport through a self-organized system should be considered. Bons & van Millingen (2001) have proposed a cellular automaton model, originally designed for heat transport in plasma experiments. The model consists of a row (N=100) of cells with pistons, that are pushed up by the fluid inside the cells and down by the springs (Figure 7). The fluid transport between cells is managed via two channels: a diffusive channel, where transport is controlled by the pressure gradients between the neighbouring cells and the permeability of the channel; and a ballistic channel, which contains a valve, that opens at a critical pressure difference P between the cells and closes at 0.1 P. Fluid is added in small amounts to random cells and it is leaving the system at one open end. As long as the pressure differences are below P, the fluid is transported through diffusive channels and transport can be described by Darcian law. If the filling rate is increased, the critical pressure differences may be exceeded between some cells and transport through ballistic channels will be activated. The transport is no longer continuous, but intermittent and occurs as bursts with amplitudes of all scales. The fluctuation of the pressure, measured in

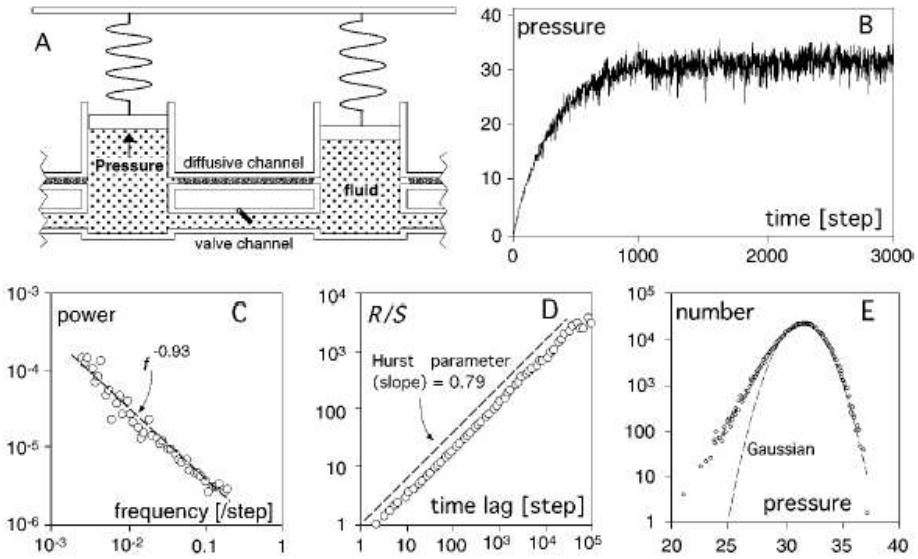

Figure 7. The piston model of self-organized critical transport. A- A fragment of the row of cells, interconnected via diffusive and ballistic channels; B- pressure fluctuation in the cell N=50; C- 1/*f* power spectrum of the pressure fluctuations; D- self-similarity analysis of the pressure; E- probability distribution function of pressure fluctuations (Bons & van Millingen, 2001).

one of the cells, exhibits a 1/*f* power spectrum, characteristically to the self-organized critical state. In that state, only average flux through the system can be determined adequately, the more detailed description of the transport inside the system is impossible (Bons & van Millingen, 2001).

Diffusional and ballistic transport modes are involved also in the sand pile model. One can imagine a sand pile, built on a vibrating table (P. D. Bons, pers. comm., 2002). The pile slope is controlled by the power of the shaking of the table. If sand is sprinkled on the pile, it is transported downward the slope according to Darcian law, as long as the amounts of added sand are small. The slope of the pile corresponds to the gradient and friction between the grains to the diffusion constant. If sand is added in larger amounts, diffusional transport may become insufficient for transmitting all the sand and avalanches occur again- the transport switches to ballistical mode.

Parallels between models described above and partial melting processes can be drawn. Diffusional transport of melt through pore space may occur, when a melt film network is formed between the rock grains. Exceeding the melt escape threshold, losing cohesion of the rock and transporting the melt along leucosomes is the way how the rock reorganizes itself for transmitting larger volumes of melt.

3.3 The use of fractals in geosciences

Power law size distributions are found and fractal techniques used also in geology. By following, few selected examples are presented.

Rothman et al. (1994) found scale invariant behaviour in turbidite deposits from two different environments in Kingston Peak Formation, USA and Izu Bonin Turbidites, Japan, basins with contrasting geological and sedimentary conditions and ages. The only common feature was the location of both basins in seismically active region. The thicknesses of turbidite layers measured in the outcrop of Kingston Peak and two well logs in Izu Bonin followed a power law with the exponents B=1.39 and B=1.12, respectively. Two Izu Bonin data sets with equal exponents of 1.12 represented layers from adjacent stratigraphic levels with no age overlap, although with remarkably higher deposition speed in younger series. As measurements of layer thicknesses show, higher sedimentation speed was attained rather by higher frequency than by greater volume of turbidite flows. Assuming that frequency of seismical events was approximately constant during both intervals (which, however, may not be true), there is no strong influence of earthquakes to the turbidite deposition. Higher sediment influx and critical accumulation on the shelf break is probably the direct trigger of turbidite flows. Authors concluded, that more observations are required to see: a) is the scale invariance generic in turbidites; b) if so, then the variation of the exponent from one region to another may be a useful indicator of sedimentation environment; c) if the exponent is invariant and does not depend on certain depositional environment, it may suggest something very general in dynamics of turbidite sedimentation; and d) if turbidite deposition is scale invariant, deviance from power law can be used as the evidence of erosion of thin layers or amalgamation to thicker layers.

Malamud & Turcotte (1999) used fractal methods to re-examine the mechanisms of heat transport from mantle to the base of the lithosphere and to estimate the role of mantle plumes in lithosphere heating. Earlier plume studies gave the plume heat flux only 15% of the total heat flux associated with the basal heating. The remainder was attributed to the secondary mantle convection or to plumes, that have insignificant expression on the surface. The cumulative frequency-heat flux distribution of 43 previously reported hot spots in the range from 308×10^9 W (the largest, Hawaiian plume) to 12×10^9 W, can be approximated to power law with the exponent 1.47. Moreover, the result is concordant with the thermal convection in the mantle, which clearly exhibits turbulence that often

satisfies self-similarity and power law statistics.

The power law distribution was extrapolated to smaller plumes, in order to estimate the total plume heat flux. About 5200 plumes with fluxes from 10^9 W were needed to cover the remained 85% of basal heating of the lithosphere. The evidence of up to 70 000 sea mounts taller than 1 km solely on Pacific plate suggests, that it is reasonable to attribute the entire basal heat flux to mantle plumes.

Clark et al. (1995) studied a network of up to centimetre wide quartz veins, arranged in brittle-ductile shear zones in Kodiak Formation, Alaska. Measured vein thicknesses followed a power law with exponent of D=1.33. Observation of the vein microtextures indicated the growth of veins by multiple events of cracking and sealing and progressive evolution from crack-seal to euhedral quartz growth with an increase in the duration of time when the cracks remained open. Initial fractures occurred due to shear stresses and were filled up by metamorphic fluids. The sealing of cracks started at crack tips, whereas fluid accumulated in the wider central part. Progressive accumulation of fluids caused the refracturing of already sealed veins and formation of new crack-seal bands, as well as the increase of time during which the larger veins as fluid reservoirs remained open. As this enhanced preferably the growth of larger veins, it acted as positive feedback in vein growth. In the extreme case, the positive feedback process may have led to fault nucleation.

Stochastic models were developed in order to investigate the dynamics of the vein growth. Models showed, that a power law vein size distribution, characteristic to Kodiak Formation, can be produced by a constant generation of veins at a proportional growth rate, whereas constant generation and constant growth give an exponential distribution. One vein birth event per 100 cracking/sealing events and 0.5% of growth in one step were appropriate parameters to generate the power law distribution with the exponent of 2.02, close to that observed in Kodiak veins.

Power law thickness distributions are found in mineralized veins, associated with ore deposits of Au, Cu, Sn, W, Pb and Zn (Roberts et al., 1999). Measurements of vein thicknesses in Castello Branco, central Portugal and La Codosera, western Spain suggested their distribution according to power law with the exponents D=0.6-1.3 and D=1.1-1.5, respectively. Lower distribution exponent was correlated with the higher gold

grade in La Codosera. A conceptual model for the development of a vein network was constructed. Vein systems initiate due to the opening of the isolated fractures. At this stage only locally derived fluid can enter the fractures and fluid migration is negligible. As veins grow, a threshold is reached, where a connected network is formed throughout the rock. This allows fluids to migrate over increased lengths and external fluids to enter the system. Transported fluids carry dissolved ore minerals, which will be precipitated by suitable conditions and will produce ore deposits.

Connected vein networks were characterized by low power law exponents, as suggests the data collected by the authors. Lower exponent indicates higher relative significance of the larger veins, that extend over long distances, therefore fluid migration and ore mineralization are enhanced in low-exponent vein systems.

In different types of volcanic rocks, both power law and exponential vesicle size distributions have been observed. Relying on the computer simulations and analogue experiments, Blower et al. (2001) suggested, that power law distributions are formed by continuous nucleation of vesicles, when successive nucleation of new bubble generations takes place in the melt pockets between the existing bubbles. As bubbles grow, the surrounding melt will be depleted in volatiles, therefore melt pockets, as less depleted regions, are favourable places for further bubble nucleation. Such process is enhanced in viscous magmas, where diffusion of volatiles is not rapid enough to maintain the equilibrium between the gas pressure in vesicles and melt. As the computer simulations show, the vesicle size distribution is greatly influenced by the number of nucleation events, i.e. the number of bubble generations formed by progressive nucleation. Low nucleation numbers apparently generated exponential distributions, whereas 5 or more nucleation events led consistently to the power law distributions.

Unlike the non-equilibrium degassing model of Blower et al. (2001), competitive theories are usually based on the assumption, that degassing is an equilibrium process.

Armienti & Tarquini (2002) analysed olivine crystal size distributions in lithospheric mantle xenoliths, sampled in different geological contexts.

Analysis of crystal sizes in thin sections suggested their distribution according to power law with the exponents of 2.4-3.8, in the size range of 0.2-25 mm. As the size distribution is the result of the disaggregation of the crystals due to high tectonic stresses, a

fragmentation model was evaluated for providing an interpretation of observed scale invariance. If grains are ordered in size classes and 80% of grains from each class are disrupted to the size of next order, the resulting exponent of the grain size distribution is 2.58, as found also in natural samples. Higher exponents (>3) can be interpreted as a result of selective crushing of larger grains and recrystallization of smaller neoblasts.

As olivine is an essential constituent of the upper mantle, its crystal size distribution determines the rheological properties of the mantle. The mean olivine crystal size is a fundamental parameter in many rheological models of the mantle. However, the observed scale invariance suggests, that mean value cannot be defined, that should be taken into account in mantle behaviour modelling. Also, the large fraction of grain boundary area, which is important in re-equilibration of fluids percolating the mantle, is associated with smaller grains, which contribution should not be underestimated.

In conclusion, some features of power law and possibilities of using the fractal methods can be shortly summarized as follows:

1) power law distributions can be described by one number - the power law exponent;

2) depending on the exponent, most of the total mass may reside in the few largest objects, or in contrary, remarkable mass can be attributed to the small, but abundant objects, the number of which may often be underestimated;

3) based on the power law extent over several orders of magnitude, the trend can be extrapolated in both directions, so the number and size of the objects, that stay beyond the observation limits can be predicted;

4) carrying out of analogue and numerical experiments to generate similar distributions in order to investigate the dynamics of processes.

4. FRACTALS IN MIGMATITES

4.1 Geological setting of investigated areas

Estonian basement

The crystalline basement of Estonia, which belongs to the Svecofennian Domain is divided into two major parts - North-Estonian amphibolite facies and South-Estonian granulite facies complexes, which are separated from each other by Paldiski-Pskov shear zone (Puura et al., 1983). Within these units, six petrological-structural zones can be distinguished - Tallinn, Alutaguse, Jõhvi, West-Estonian, Tapa and South-Estonian zones, each of them with different composition and metamorphic grade (Figure 8).

The Tallinn zone is characterized by the amphibolite facies metavolcanites and metasediments of Jägala complex - amphibole gneisses, biotite-plagioclase gneisses, quartz-feldspar gneisses, mica gneisses, and minor sulphide-graphite gneisses and magnetite quartzites. The migmatization is common (Soesoo et al., 2004 a).

The main rock types of the Alutaguse zone, metamorphosed generally in amphibolite facies are Al-rich gneisses containing biotite, cordierite, garnet, and sillimanite, and biotite-plagioclase gneisses. Also, less abundant amphibole gneisses, amphibolites, and quartz-feldspar gneisses occur. Within the zone, Sonda-Uljaste and Assamalla domes exhibit higher, granulite facies metamorphism and comprise of sulphidic black schists, quartzites, skarned carbonaceous rocks and pyroxene gneisses. The migmatization is widespread in the Alutaguse zone (Soesoo et al., 2004 a).

The Jõhvi zone, metamorphosed under conditions of granulite facies, is composed of rocks of the Vaivara complex- pyroxene gneisses, quartz-feldspar gneisses, biotite-plagioclase gneisses, amphibole gneisses and garnet-cordierite gneisses. Al-rich gneisses and magnetite quartzites occur in limited area; the quartzites cause the Jõhvi magnetic anomaly. Granitic and charnockitic migmatization is widespread (Soesoo et al., 2004 a).

The West-Estonian zone consists predominantly of biotite-amphibole gneisses, amphibolites, biotite-plagioclase gneisses and quartz-feldspar gneisses, with minor pyroxene gneisses. The metamorphism has undergone at high-temperature amphibolite facies, in some places at granulite facies. Granitic and placioclase- potassium-feldspar migmatites occur in amphibolite facies areas, in areas of granulite metamorphism, migmatites of enderbitic composition are common (Soesoo et al., 2004 a).

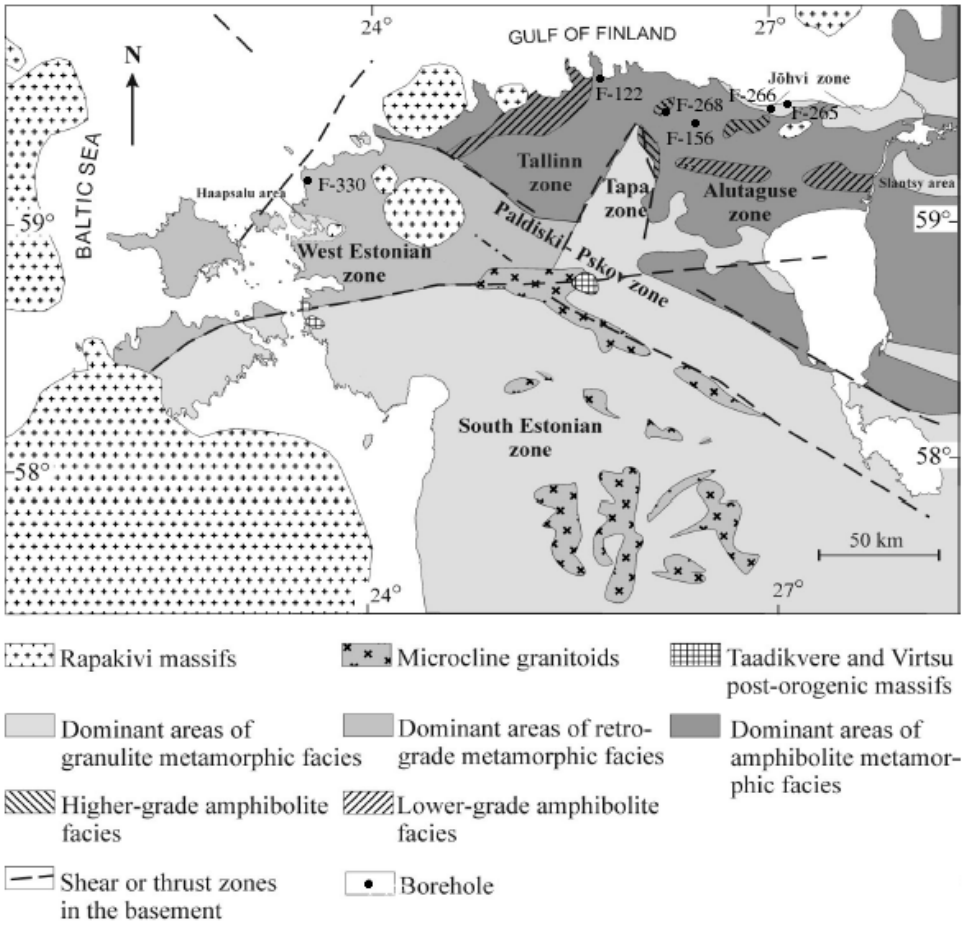

Figure 8. Map of the crystalline basement of Estonia. Modified from Puura et al. (2004). The locations of boreholes studied in this work are shown.

In the Tapa zone, a rock association, analogous to that of the West-Estonian zone occurs (Kivisilla et al., 1999). The traces of granulite metamorphism have probably been partly overprinted by high temperature retrograde metamorphism (Koistinen et al., 1996). Granitic and potassium feldspar- plagioclase migmatites dominate, charnockitic veins prevail in the areas of granulitic metamorphism (Soesoo et al., 2004 a).

The South-Estonian zone, metamorphosed in granulite facies is characterized by hypersthene, pyroxene and amphibole gneisses, originating from mafic to intermediate volcanics and greywackes. Pyroxene gneisses, that have undergone granitic and charnockitic migmatization are characteristic of that zone (Kivisilla et al., 1999).

According to the geothermobarometry, the temperature and pressure estimates for the South-Estonian granulite facies complex are 700-800 ºC and 5-6 kbar, respectively; for the North-Estonian complex with lower metamorphic grade, the estimates are 600-700 ºC and 3-5 kbar (Koistinen et al., 1996). Peak metamorphic conditions of the South-Estonian complex, higher than characteristic of Svecofennian metamorphism suggest much deeper erosional level compared to the North-Estonian amphibolites (Puura et al., 2004).

Age determinations by U-Pb isotopic analysis have suggested the age of 1.83 Ga for the South-Estonian granulites (Petersell & Levchenkov, 1994). South-Estonian granulites have been compared to the Haukivesi-Kiuruvesi complex in Finland, the metamorphism of which is dated at 1.88 Ga (Koistinen et al., 1996). However, relying on the new age data, Puura et al. (2004) argued, that granulite facies metamorphism is distinct from that in southern and central Finland. The age of the metamorphism for West-Estonian metavolcanics is dated at 1.83 Ga, for Tallinn zone metasediments at 1.8-2 Ga and for Tapa zone 1.92 Ga (Petersell & Levchenkov, 1994). The North-Estonian amphibolite complex is regarded as an extension of the respective rocks of southern Finland with metamorphism at 1.81-1.83 Ga ago (Koistinen et al., 1996).

Masku, southwestern Finland

The migmatites of the Turku area are part of the southern Svecofennian Shist Belt (sSSB), which forms the southern area of Svecofennian domain in Finland and southeastern part of Sweden (Figure 9). This 1.8-2.0 Ga old crustal segment consists of calc-alkaline intrusions and metavolcanics, intercalated by metagreywackes and -pelites. Three larger areas with higher granulitic metamorphism grade can be distinguished in sSSB- the Turku Migmatite Complex, the West Uusimaa Granulite Complex and Sulkava Granulite Complex, which have undergone similar thermo-tectonic evolution. U-Pb age determinations of metapelitic

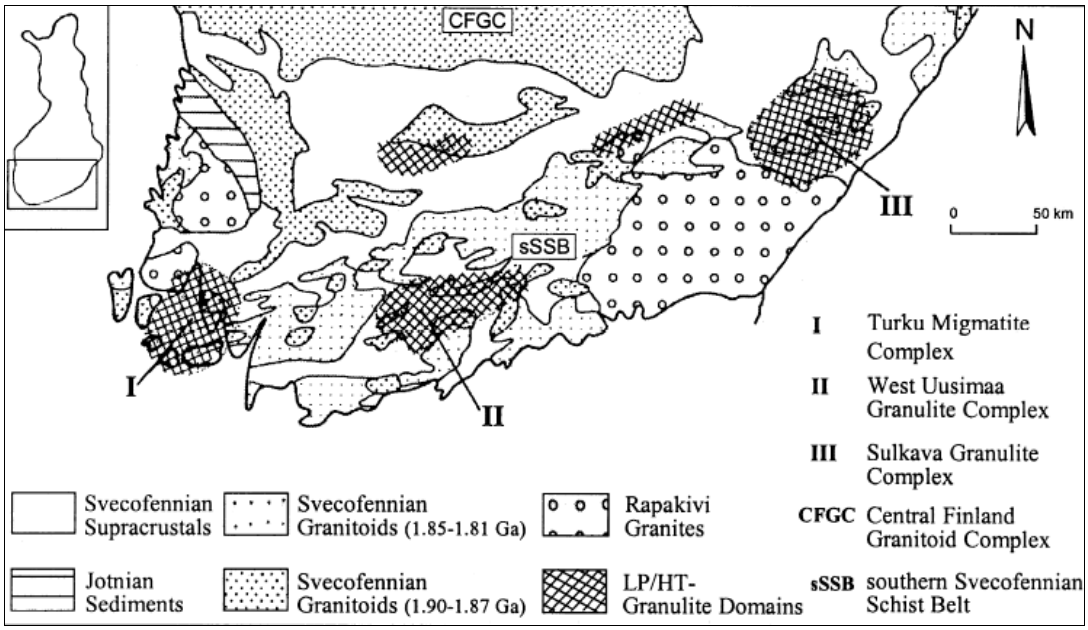

Figure 9. Geological sketch map of southern Finland (Mengel et al., 2001).

migmatites and S-type granites of the Turku area resulted consistently in 1.83-1.84 Ga (Mengel et al., 2001).

Investigated migmatites are located about 15 km northwest from the Turku in Masku village, where several outcrops are available for observation. The typical lithologies of Turku migmatites are plagioclase-quartz-biotite gneisses, metapelitic mesosomes with abundant *in situ* leucosomes, potassium feldspar-plagioclase-quartz leucosome sills and composite leucosomes with melanosomes rich in biotite, garnet and cordierite (Mengel et al., 2001).

Montemor-o-Novo, central Portugal

The migmatites studied near Montemor-o Novo town in central Portugal belong to the Evora Massif which is included in the northwest-southeast directional Ossa Morena Zone, passing through Portugal (Pereira & Silva, 2002).

The Hesperian Massif, which occupies the western and central part of Iberia, is a fragment of Variscan basement (Figure 10). Several terranes of various origins have been accreted to the Hesperian Massif during Variscan Orogeny, with Iberian terrane constituting most of the Hesperian Massif area. The Ossa Morena Zone, the southwestern part of the Iberian terrein, consists mainly of preorogenic metasediments- the Serie Negra Group of Middle and Upper Riphean age, overlying a metaigneous and -sedimentary succession of gneisses and amphibolites of unknown age. These sequencies have been deformed during the Cadomian Orogeny (Moores & Fairbridge, 1994). The age of the metamorphism of the Montemor-o-Novo high-grade metamorphic terreins, developed on the Serie Negra succession, is poorly understood due to insufficient geochronological works. It can be of Variscan age or alternatively, Cadomian age like some other high temperature/low pressure tectonothermal events in the Ossa Morena Zone (Pereira & Silva, 2002).

The Montemor-o-Novo migmatites are available at the 200 m long Almansor river section. These are sheared migmatites with very high fraction of melting, which gradually pass into tonalite massif few hundred metres northwest. In addition to the leucosome (consisting of quartz + potassium feldspar + plagioclase ± biotite,muscovite, sericite, cordierite) and melanosome (biotite + plagioclase + quartz + sillimanite + garnet) layering amphibolitic enclaves or rock fragments from the SerieNegra Group are present, that have resisted the migmatization (Pereira & Silva, 2002).

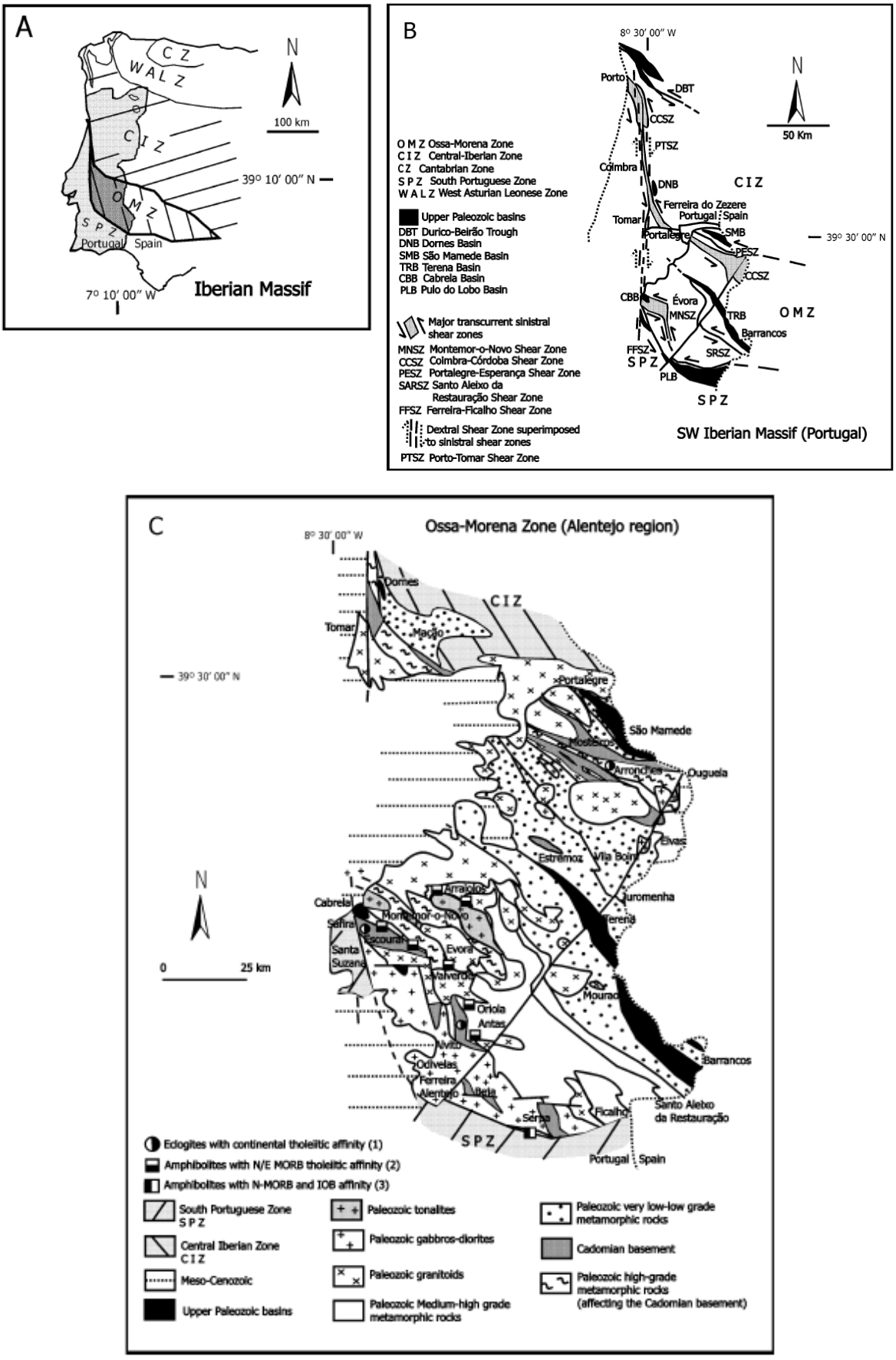

Figure 10. A- Subdivision of Iberian Massif into zones and location of Ossa-Morena zone. B- Geological sketch map of SW part of Iberian Massif. C- Geological sketch map of Ossa-Morena zone in Portugal (Silva & Pereira, 2004).

4.2 Measurements of leucosome widths in migmatites

In drill cores and outcrops the thicknesses of leucosomes and their spacing along line traverses were measured (Figure 11). The resolution of measurements was limited to 2 mm, leucosomes with thicknesses below this value were not counted as their number would be very likely underestimated and should thus not included in the data.

The drill core usually penetrates the migmatite layering at an angle, the same occurs in outcrops where regardless of placing the measuring traverse perpendicular to the layering, the erosional surface may cut the leucosomes at some angle. Therefore apparent thicknesses are in fact measured in most cases. As the apparent thicknesses differ from real ones proportionally, the thickness distribution statistics remains unaffected.

One problem with measurements of leucosome thicknesses is the discontinuity of the drill cores and outcrops, which makes it impossible to count all the leucosomes residing in the observable section. The missing sections, however, may have contained large and small leucosomes with the same probability as in available parts, thus not decreasing the reliability of the data. It could be problematical to determine the fractal dimension by box counting method (described below), which becomes meaningless when large parts are missing from the measurable section.

The leucosome fraction in migmatites was estimated, which however, does not reflect the melting rate of the migmatite, as the amount of extracted or injected magma in the observable block cannot be determined. As a large fraction of melt may reside in the smallest leucosomes, which remain under the resolution limit, the leucosome fraction describes rather the minimal amount of magma in the migmatite.

Figure 11. Measurement of leucosome widths in a drill core from the Estonian basement.

Below, the drill cores and outcrops, where the measurements were performed are described, as well as the position of sample sections, the number of measured leucosomes and the dominating rock type inside the section are shown. Localities of the studied drill cores are also shown on the map of the Estonian basement on Figure 8.

F–156 Ubja, Alutaguse zone. In a section of 252–292 m 450 leucosomes and granitic veins in the width range of 3…635 mm were measured. The main rock type in the studied section by Kivisilla et al. (1999) is biotite-plagioclase gneiss.

The data is collected by A. Soesoo and P. D. Bons.

F–265 Tõugu, Jõhvi zone. In the depth range of 270-364 m 548 granitic veins and leucosomes with thicknesses of 2…2627 mm were measured.

Main rock types are pyroxene amphibolites and biotite-plagioclase gneisses (Kivisilla et al., 1999).

Data is collected by A. Soesoo and J. Kirs.

F-266 Nudi, Jõhvi zone. 578 leucosomes with thicknesses of 2…515 mm were measured in a depth range of 228-282 m. The drill core penetrates biotite-plagioclase gneisses in the studied section (Kivisilla et al., 1999).

F-268 Vanamõisa, Alutaguse zone. 248 veins with thicknesses of 2…6152 mm were measured in the depth range of 368-418 m. Syenogranites and amphibole-pyroxene gneisses dominate in the section (Kivisilla et al., 1999).

F-122 Aabla, Tallinn zone. In the section between 169-195 m 102 leucosomes in the width range of 2…1214 mm were measured. Main rock type: amphibole-biotite gneisses (Kivisilla et al., 1999).

F-330 Elbiku, West-Estonian zone. 105 veins with thicknesses 2…2077mm in a section between depths of 250-289 m were measured. The rock type is syenogranite (Kivisilla et al., 1999).

Montemor-o-Novo outcrop. 713 leucosomes in the thickness range of 2…1805 mm were measured along a 42 m line traverse.

Masku outcrop. On a 5 m long line traverse 177 leucosomes with thicknesses of 2...135 mm were measured.

As plotted on a bilogarithmic graph, measured leucosome thicknesses follow the power law in most migmatites (Figure 12). Different methods can be used for plotting the power law data on the graph. The cumulative distribution represents the number of leucosomes, whose thickness is greater than a given thickness. An alternative way is the density distribution, which represents the number of objects belonging to an interval, divided by the interval length dh as $N(h) = h^{-D}/ dh$ (Bonnet et al., 2001). The length of intervals, or bins, wherein the objects are distributed according to their sizes, can be constant or increase logarithmically with the increase of object sizes. In both cases, the resulting distribution exponents are increased by one (D+1) compared to the exponent D of cumulative distribution (Bonnet et al., 2001).

The disadvantage of the cumulative distribution is the suffering of curvature effect at the large scale, which is due to its logarithmical nature. As the number of largest objects approaches 1, the logarithm approaches zero, causing the steepening of the trend at the lower end. The density distribution is free of that effect as the number of objects belonging to the largest bin is increased. However, the disadvantage of the density distribution is the influence of chosen bin size to the number of objects belonging to that bin, which may lead to the decrease of smoothness of the density distribution trend (Bonnet et al., 2001).

By geologists, the cumulative frequency distribution is most commonly used, as it is easily computable and the data has not to be binned (Bonnet et al., 2001). In this work, both distributions were used for comparison. Logarithmic binning was used by the estimation of the density distribution exponent.

For adequate definition of power law exponent, values over 2-3 orders of magnitude should be sampled. The number of the objects required depends on the exponent- the higher the exponent, the steeper is the graph and the more objects are needed to define the exponent over a given scale. As a rule, minimum 200 objects are required for accurate determination of the power law exponent (Bonnet et al., 2001).

In addition to cumulative and density power law distributions, the topological dimension of migmatite structures was estimated by box-counting method, which describes the spacing of objects and corresponds to the fractality in the strict sense. In the present one-dimensional situation, sections with logarithmically increasing lengths in the range of 1-4096 mm were generated on the measured data and the number of sections containing leucosomes was counted. Only bin size power law distributions with exponents differing from integer should be referred to as topological fractals (Bonnet et al., 2001).

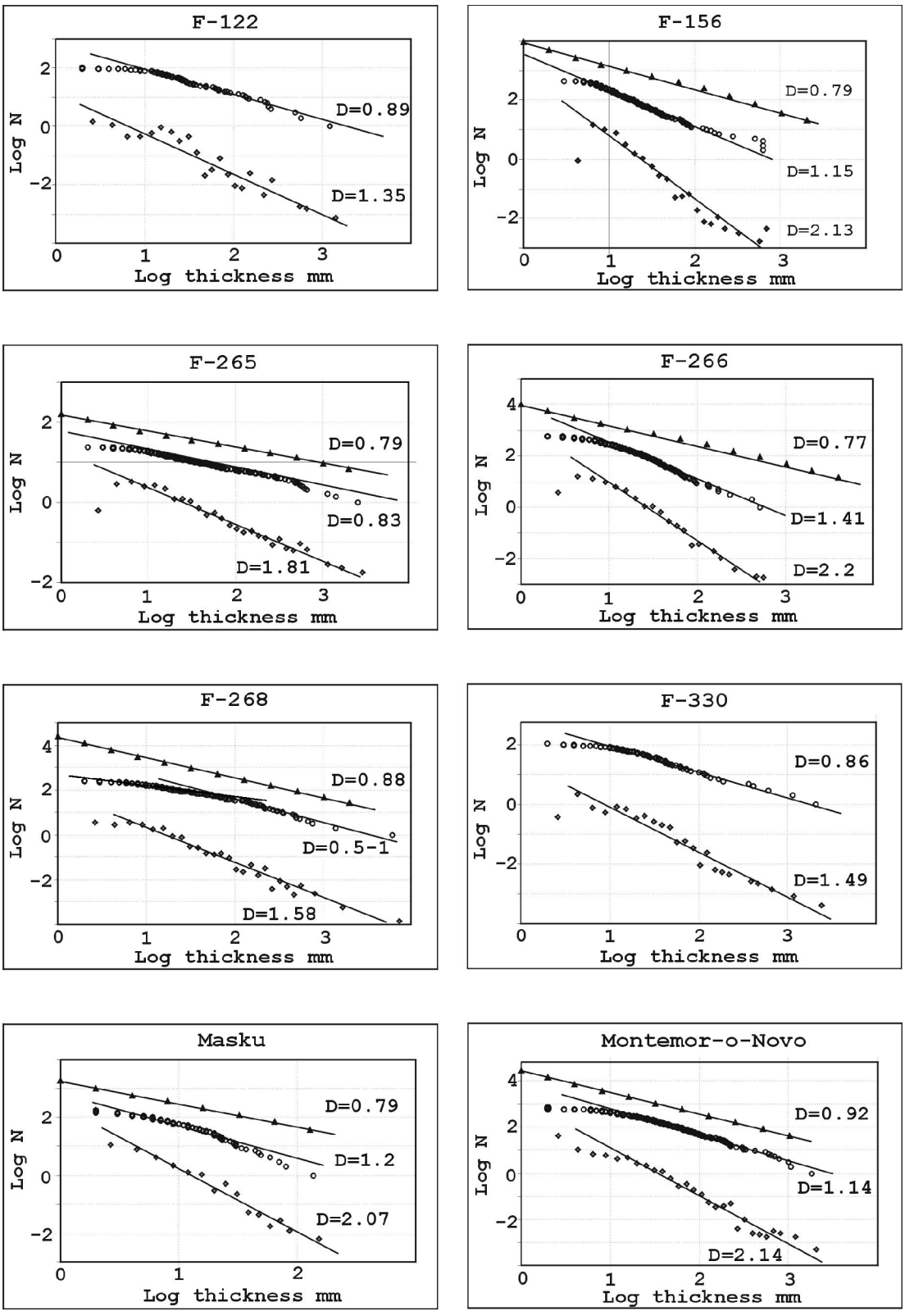

Figure 12. Leucosome thickness distributions in studied drill cores and outcrops. Squares represent density distribution, circles cumulative frequency distribution, triangles the determination of fractal dimension by box-counting method.

Locality	Metamorphic grade	Cumulative distribution exponent	Density distribution exponent	Fractal dimension by box-counting	Fraction of leucosomes, %
F-122	amphibolitic	0.89	1.35	-	23.5
F-156	amphibolitic	1.15	2.13	0.79	24.2
F-265	amphibolitic	0.83	1.81	0.79	28
F-266	amphibolitic	1.41	2.2	0.77	19.3
F-268	amphibolitic	0.5-1	1.58	0.88	44.4
F-330	granulitic	0.86	1.49	-	19.8
Masku	granulitic	1.2	2.07	0.79	39.6
Montemor-o-Novo	high, not specified	1.14	2.14	0.92	71

Table 1. Results of leucosome width distribution measurements in migmatites.

As it can be seen on Figure 12, the data of most measured migmatites fits on the power law trend with higher or lower precision. The exceptions are the drill core F-268 and Masku outcrop, which cumulative distributions may probably be better described by exponential law. In F-268, smaller and thicker veins seem to define separate trends with exponents 0.5 and 1, respectively. However, as plotted using density distribution, the power law is defined in both localities. The results of leucosome measurements are summarized in Table 1.

The variation of distribution exponents in the range of 0.83-1.41 (cumulative distribution) seems not to be related to the host rock type or metamorphic grade.

The spacings between leucosomes along the section were analysed in F-156, F-265 and Montemor-o-Novo, suggesting that they are not random but definable by the exponential law.

The deviations from the power law trend at the upper part may be a result of the underestimation of their number due to the small thicknesses. Alternatively, it has been proposed, that smaller objects can be undersampled due to their real absence in the section, as natural processes may set limits to the power law extent, thus the involved process may exclude the formation of smaller leucosomes (Bonnet et al., 2001). As the deviation occurs in migmatites already at 10 mm, the latter possibility should be considered and the uncertainities cannot be simply regarded to underestimation of the number of small leucosomes.

5. ANALOGUE MODELLING OF PARTIAL MELTING PROCESSES

5.1 Why to use an analogue material?

To investigate the dynamics of a process, that takes place in the Earth's crust, one can take a piece of the crustal material and subject it to the conditions existing in the crust. In most cases high temperatures and pressures are applied to obtain these conditions. Special and complex equipment is needed, especially for the pressure control. Also, in the case of the melting experiments, the size of the sample is limited and is in the range of few centimetres (e.g. Knesel & Davidson, 1999). Therefore only small-scale processes can be recreated and analysed. Moreover, one may want also to see what happens during the experiment. At extreme temperature-pressure conditions the direct observing and monitoring of the experiment evolution is complicated and only the end product of the process can be revealed.

These problems occur, when the sample material dictates the design of the experiment. Instead of adapting the experiment to the material, one can adapt the material to the experiment and choose a material, that enables the experiment to be performed. The behaviour of the selected material is considered to be analogous to that of the real material but without applying extreme conditions. The main advantages of analogue modelling approach are very simple equipment and possibility of real-time observations. However, one should keep in mind that the behaviour of experimental and real systems is analogous, but not identical, thus care must be taken in the interpretation of the experiment results and in application of the results to real rocks.

In this chapter, description of an experiment will be presented, that was set up to model migmatization processes in the Earth's crust, sand and carbon dioxide were used as analogue materials for host rock and melt, respectively.

5.2 Set-up and progression of the experiment.

The analogue experiment, which will be described below, was originally designed and performed by Bons & van Millingen (2001).

The aim of this experiment was to visualize fluid phase segregation processes, that may account for partial melt formation, as well as to find similarities between the behaviour of the experimental and natural systems by the comparison of the generated structures. The

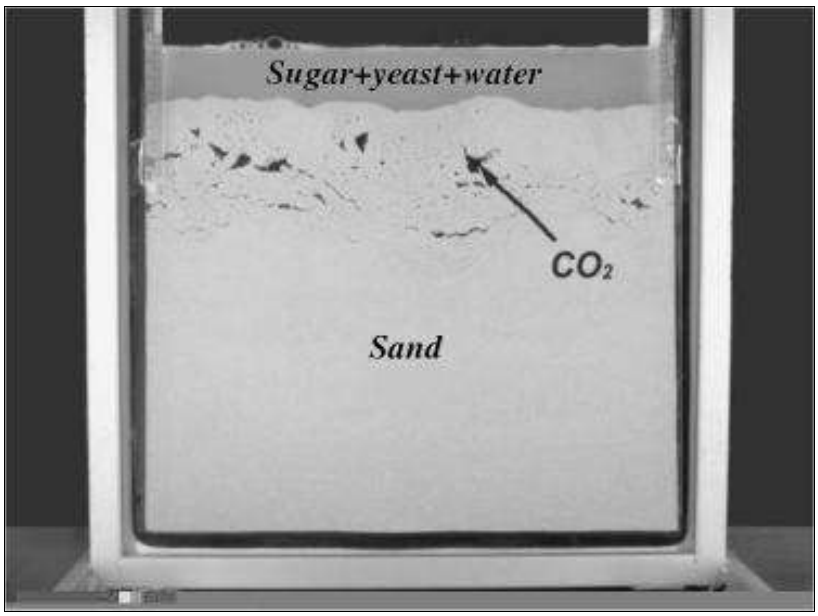

Figure 13. Set-up of the analogue experiment. Tank width is 35 cm.

experiment was also carried out for supporting the interpretations of leucosome width distributions measured in migmatites and their relation to melt formation and redistribution mechanisms in the rock.

The experiment was set up in a 35 cm-wide flat glass tank (Figure 13), which was made of two glass plates with the distance of 6.5 mm between them. The tank was filled up with fine grained (<0.25 mm) well-sorted quartz sand and a mixture of sugar solution with yeast. The sand acted as analogue of the solid phase or country rock that is undergoing migmatization. The porosity of the sand was approximately 30% and the space between the sand grains was filled with the sugar water/yeast mixture.

The life activity of yeast bacteria results in the production of alcohol and CO_2 gas, the latter was assumed to be generated at uniform rate throughout the volume of the tank. The gas production was considered to be the analogue of partial melt formation during crustal anatexis.

In order to enable further analysis of any moment from the sequence of the events, the progression of the experiment was recorded by a digital photo camera.

At the initial stage of gas formation, small gas bubbles resided in the interstitial space between sand grains. Due to the pore water and the gas density differences, bubbles were pushed upwards with a force dependent on the bubble size- the larger bubble, the stronger force (according to Archimedean law). As the gas production was low at the beginning of the experiment, diffusional transport through pore fluid was sufficient to drain all the

Figure 14.
Formation of an initial subhorizontal crack. Actual size.

formed gas. First gas accumulation batches and flow paths - subhorizontal cracks - appeared in half of an hour, when gas production reached the critical rate, at which diffusion alone wasn't satisfactory any more for the gas transport (Figure 14). The system in the tank has modified itself for transmitting larger volume of gas by opening cracks and voids as additional gas escape pathways and temporary accumulation sites. This is the evidence of switching from diffusional to ballistical transport mode. First cracks formed preferably in the upper part of the tank, where gas flow rate through pore space was highest, as well as the compressional stress caused by the overlying sand layer, which is to overcome to open a crack, was lower.

In ballistical mode, the accumulation and transport of the gas was not gradual, but intermittent and occurred stepwise. The distribution and transport of the gas phase was managed by the merging of the batches, as voids grew bigger and became connected (Figure 15), or by draining the gas from one part of the tank into another. Resulting batch grows until a critical volume was achieved that created enough buoyancy to rise it to the surface and escape from the system. The escape occurred as sudden gas bursts with subsequent collapse of the voids. Larger batches are more forced upwards and have thus bigger potential to carry the gas out of the system, although at suitable conditions also smaller batches are able to reach the surface. In the originally performed experiment, Bons & van Millingen (2001) reported the power law distribution of escaping gas batch volumes, and accordingly the largest, but rare batches accounted for the most of the escaping gas volume. The velocity of the ballistic transport was considered to be several orders of magnitude greater than in diffusion mode.

The movement of gas in the experiment was controlled by gas pressure gradients- the gas tends to flow towards lower pressure. The draining of one void into another and/or gas escaping results in redistributing of the pressure throughout the volume of the tank. As the result, new batches get mobile. Any gas movement at the one edge of the tank may trigger an event at the other edge. In this way, a “communication” can exist between different

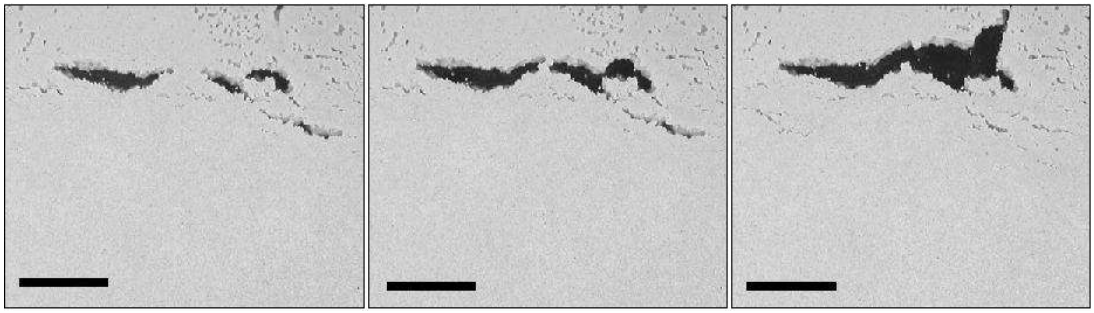

Figure 15. Merging of gas batches. Scale bar is 28 mm.

parts of the system. Using this "communication", the system organizes itself in the state, where the size of gas escape events shows power law distribution and gas level fluctuation in the system is 1/*f* noise, which means that the gas transport in the tank is of self-organized critical nature (Bons & van Millingen, 2001).

The behaviour of the experimental system is analogous to models of self-organized critical systems described previously in the chapter 3.2. At low transport rates, diffusion is sufficient to transfer all the matter needed. To transmit large amounts of the matter, the system has to modify itself and use alternative faster transport mechanisms: avalanches occur on the sand pile and ballistic channel valve is opened in the piston model. These events are comparable with the opening of the cracks and voids and the following rapid expulsion of the gas in the analogue experiment.

The stepwise accumulation of gas in the crack-shaped voids occurred during the first hour of the experiment. At later stages, a static network of the bubble-shaped voids was developed, providing an steady open escape path for the gas over a long time period. This was probably due to the cohesion between sand grains and limited compression effect of the overlying sand that avoided the closure of the drained voids; as well as by complete mixing of the system during the continuous gas production and transport (Bons & van Millingen, 2001).

5.3 Analysis of experiment results

To enable the later analysis of the processes, the development of the experiment was recorded with a digital photo camera with a 5.5-second interval during approximately one and a half hour. Further closer study was concentrated on the first 40 minutes of the experiment. In this period the stepwise transport of gas in the crack-shaped voids dominated and only minor influence of static structures described above was observed.

Pictures were analysed on the computer using the ImageJ image processing software

(available as freeware at the website rsb.info.nih.gov/ij/), that enables measuring of object's dimensions and other parameters on images. The aim of the analysis was to estimate the quantity of the gas in the tank along the time series, as well as the size distribution of the gas batches in some selected time steps. The measurements of gas batch sizes along a line analogously to the leucosome width measurements in migmatites could not be performed, due to the lack of statistical material, as few batches would fall on the vertical measurement line. Therefore, sizes were estimated as the batch areas in two-dimensional situation.

On a thresholded image, the area in pixels of every single batch was measured (Figure 16). Images had a resolution of 72 pixels per inch, sufficient to measure the objects with sizes of one millimetre and less. The total of gas in the tank was then derived by total sum of batch areas. The structure on the measurable image must be treated as a 2-dimensional cut through 3-dimensional voids spatially distributed in space. The estimated gas amount corresponds to the total area of the visible cracks and voids, and not to the volume of gas in the system, regardless of the flatness of the tank. The gas residing in the pore space was also not taken into account.

As plotted on the log-log diagram, the cumulative distribution of the gas batch sizes obeys the power law with an exponent about 0.5 over almost three orders of magnitude (Figure 17). The measurements of batch sizes at different time steps show that data fits quite well the power law continuously throughout the experiment. However, the distribution exponent is variable and increases gradually from 0.5 at the beginning of the experiment to nearly 2 after 1.5 hours. The record of the gas amount fluctuations, as well as long-term variation of the distribution exponent during the experiment are presented on Figure 18.

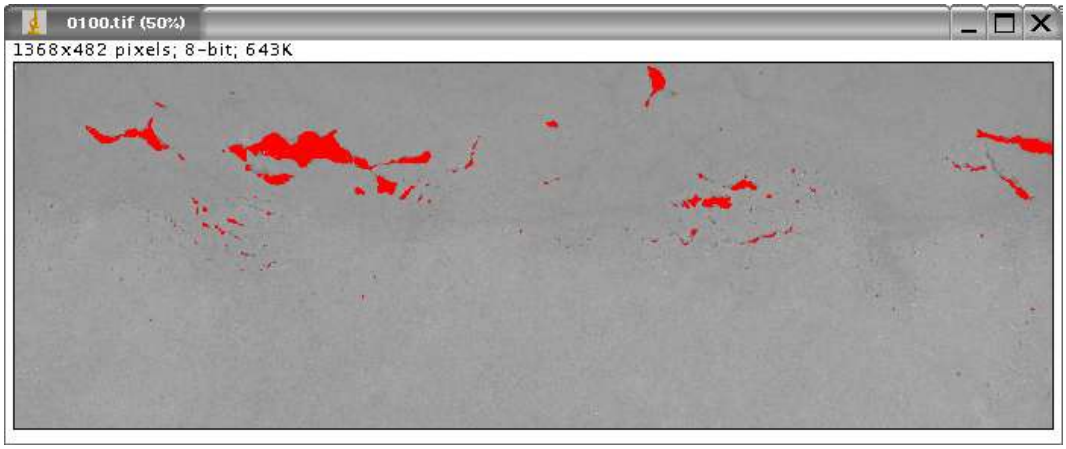

Figure 16. Measurement of gas batch sizes on a thresholded image. Red areas were counted.

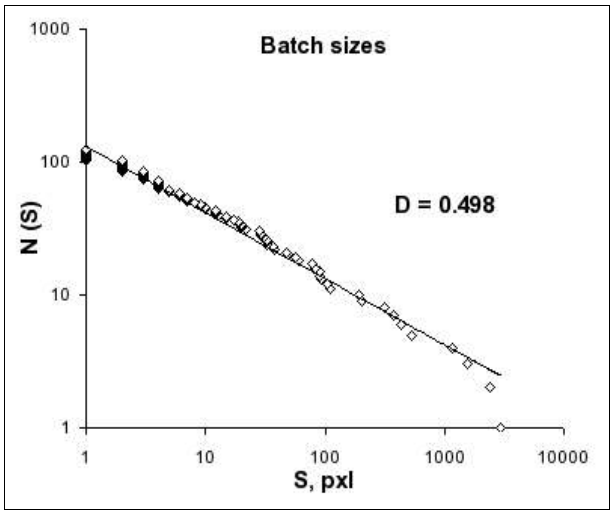

Figure 17.
Cumulative distribution of gas batch sizes about 8 minutes after the first crack appeared.

The total gas amount fluctuated in the range from 7000 to 17000 pixels in the first part of the experiment, which corresponds to 1 to 2.6 % of the gas fraction residing in the open cracks if compared to the image area.

The question is, how the observed gas batch size distributions with particular exponents are related to the gas segregation and transport dynamics, i.e. are they affected by processes of gas accumulation or escaping from the system? In order to determine this, the study was focused on a time period, where remarkable changes occurred on the gas quantity in a short time (Figure 19). On selected images, size distributions and distribution exponents were estimated and compared with each other, to find their possible local fluctuations depending on gas movements.

One would expect that accumulation of the gas in the tank results in the increase of the relative significance of larger batches and thus lowers the distribution exponent. The gas escape on the contrary would cause the exponent to raise as larger voids will collapse and disappear. However, as it is evident from the Figure 19, short-term processes or single events of gas phase segregation do not have considerable effect on the development of the distribution exponent. Even in the case of rapid discharge of the system, when more than 50% of the gas is escaping the tank in few seconds, the exponent remains unaffected. Draining off the gas by the few biggest batches, that contain a large fraction of the gas in the system seems to cause rather a little bend-off from the power law trend in the lower part of the distribution than affect the whole data. In the same way, accumulation seems not to have any influence on the value of the exponent. Apparently negligible changes in exponents can probably be attributed to the long-term increasing trend and possible inaccuracy in exponent determination.

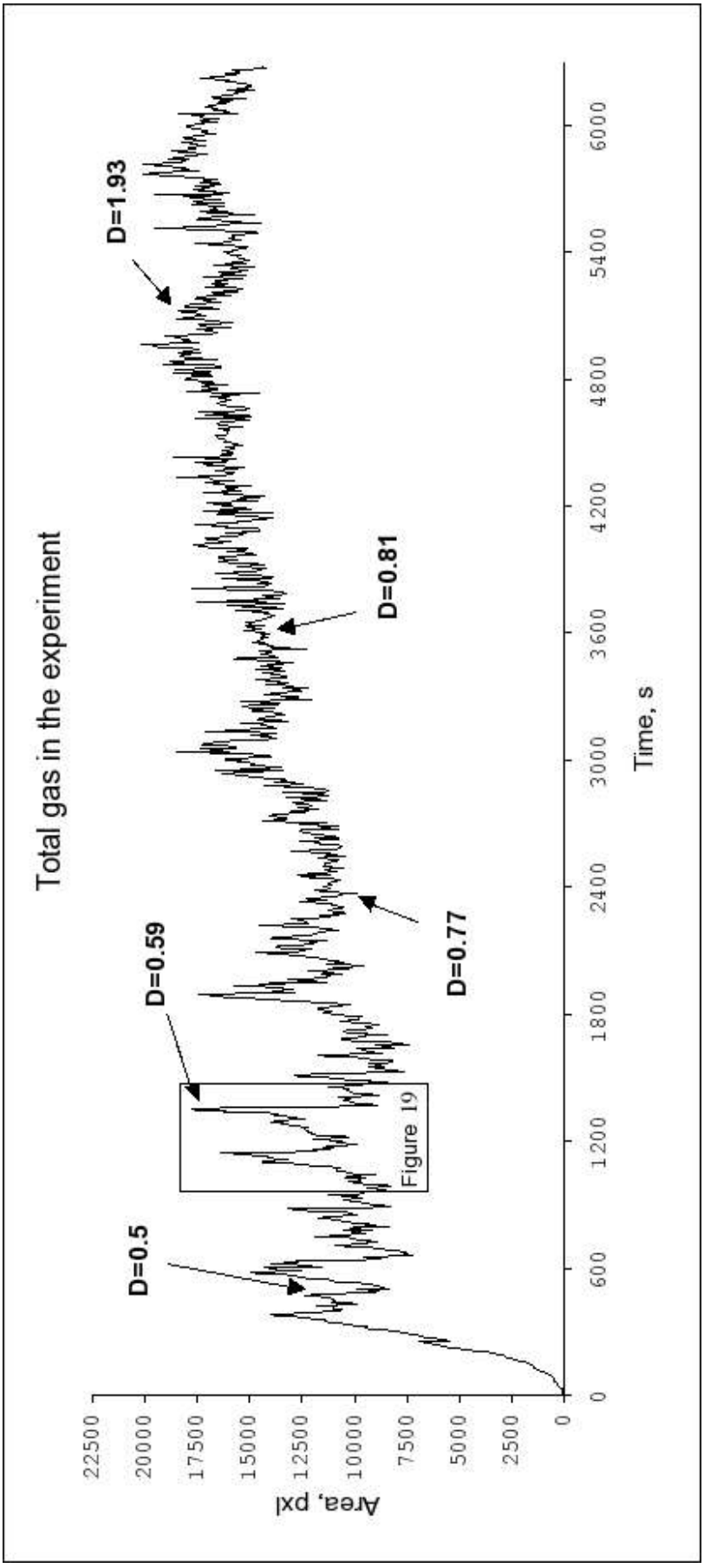

Figure 18. Fluctuation of gas amount and variation of batch size distribution exponent during the experiment. The area in the rectangle will be presented on the Figure 19.

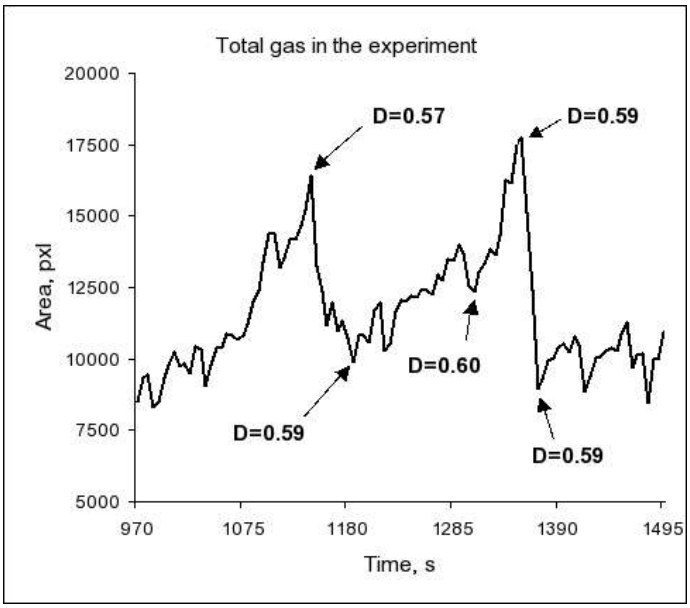

Figure 19.
Close-up to the gas fluctuation signal in the range of 16 to 25 minutes. The power law exponents of gas batch size distributions at selected time steps are displayed.

The gradual, but steady gain in the exponent throughout the experiment is rather the result of the incomplete closure of the drained voids and static void network formation, than a progressive development of the system in the state with the higher exponent of the batch size distribution, caused by gas segregation and accumulation processes. Bubble-shaped voids, that stay open, are preferentially small and increase therefore the significance of the smaller batches in the distribution, which in turn gradually raises the exponent. The described behaviour of sand is an evidence of the imperfectness on using it as analogue material for the rock and will obviously somewhat affect the reliability of the experiment results.

As far as the influence of static behaviour of sand becomes more important with time, reliable results should emerge rather at the incipient stage of the experiment, where discontinuous transport of gas by merging and draining of the crack-shaped voids was dominant. For this time, the system has already developed into the state, where power-law batch size distributions occurred. Therefore, power-law exponent of 0.5-0.6 should be the value that describes the gas accumulation and transport in the tank, regardless the misbehaviour of sand as analogue material.

6. DISCUSSION

6.1 Numerical melt segregation and accumulation model

The analogue experiment conducted in this study suggested the emergence of fractality similar to migmatites and consequently, the possible relationship of processes invoked in both analogue model and crustal melting can be discussed. Final decisions, however, are hard to make solely on the basis of the analogue experiment. A numerical model can provide valuable supportive information for interpretation of the data gathered during the analogue experiment as well as the observations in nature.

Few attempts have been made to model the partial melt processes numerically (e.g. Vigneresse & Burg, 2000, Bons et al., 2004). The following presents a model of Bons et al. (2004). This model describes the melt segregation and accumulation in combination as a discontinuous process, that is of self-organized critical nature and explains the development of the resulting fractality. Such a model can be helpful for understanding fractal structures and related dynamics of melt transport in migmatites.

The concept of the model is that the initial melt, segregated from the grain boundaries resides in the discrete veins. Veins grow and new veins form by progressive melting, eventually neighbouring veins can reach to each other and merge into one bigger vein. The interaction of veins is enhanced by mobility, which is caused by deformational stresses. As veins grow, buoyancy forces become dominant and thus enable the larger veins to escape the system, draining them to the upper level or ascend through the crust to the surface.

In the numerical model, melt veins were designed as spheres. Progressive melting was simulated as the succession of the cycles. Typically 5000 cycles were passed in the experiment. In each cycle, the model went through the following steps (Figure 20). First, the formation of the initial melt was performed by adding the spheres of the unit size randomly into a 100x100x100 unit cube. 100 spheres, i.e. 0.01% of melt was added in each cycle. In the second step, melt batch migration was simulated by moving all batches independently to their size in a randomly chosen direction, moving distance was dependent on the mobility factor E and was a random number in the range of $\pm$ E.

Next, the possible overlapping or touching of spheres was checked. Such spheres were merged into a new larger sphere, with the total volume of the merged spheres and with the position as volume-weighted average of their centres. All spheres, that exceeded the

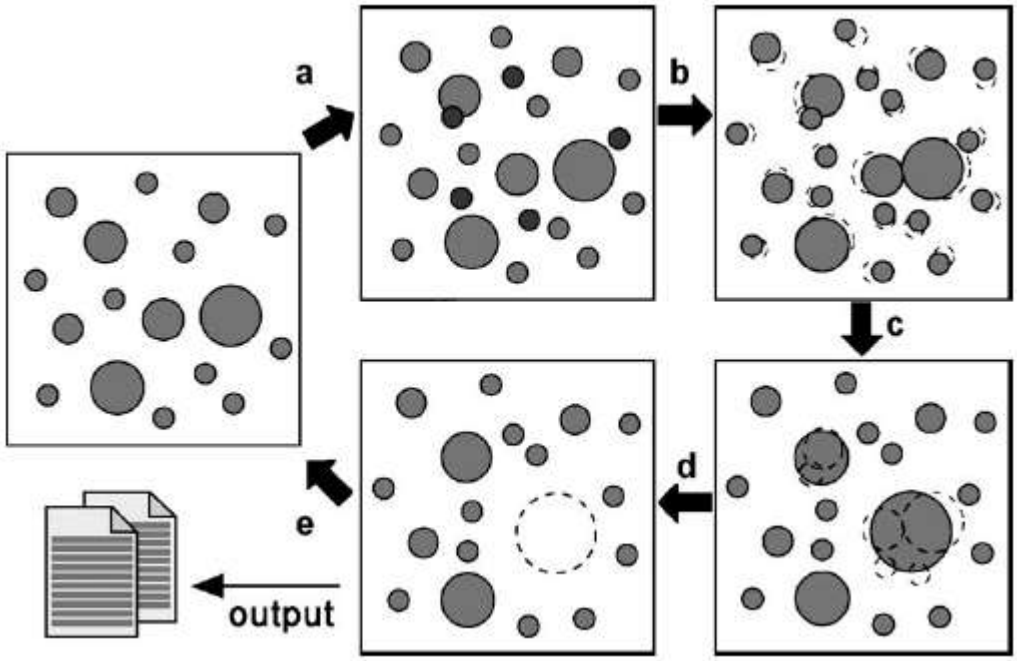

Figure 20. Numerical melt segregation and accumulation model : a) adding new spheres of unit volume; b) movement of all spheres according to mobility E; c) merging of overlapping spheres; d) removing of batches, that exceed the critical volume; d) recording the data and start of new cycle (Bons et al., 2004).

critical volume V_{max} (typically V_{max} =2000 in the experiment), were removed from the cube at the next step, corresponding to the melt extraction. Preferred upward propagation of the spheres as melt transport by buoyancy forces was not included in the model.

In less than 200 cycles, the experimental system reached a dynamic equilibrium, where the melt extraction was equal to its addition, but only in long-term average. The size of the extracted batches varied from the critical extraction volume to approximately 8000, when several large batches merged prior to extraction. Extracted batch size distribution according to the power law with the exponent of 3.2 indicates possible achievement of self-organized critical state. Once this state was established, the system was able to discharge any amount of melt without further modifying itself- the volume distribution of spheres inside the cube remained constant and followed the power law with the distribution exponent varying between 2/3 and 1, depending on the mobility rate E. In case of high mobility of spheres (E≥4), the distribution exponent approximated to 2/3, meaning that most of the mass resided in the few largest spheres with the largest one containing half of the volume, therefore suggesting effective accumulation. If spheres were not moved (E=0), the exponent was close to 1, suggesting poor accumulation. The power law with the exponent of 1 represents the situation, where equal volumes reside in each

volume category, i.e. batches with the volumes of 1 to 10 contain the same total mass as the batches with the volumes in the range from 10 to 100, and so on. Thus, most of the mass resides in small spheres. The exponent value of 1 can be treated as a boundary between accumulation and dispersion of the melt.

Besides good accumulation, also high mobility enhances melt extraction, as the critical size of spheres is reached faster, which causes earlier onset of their extraction from the system. As well, mobility was effective on the average melt fraction and the number of spheres in the cube, ranging from 2.6% and 5000, respectively if E=0, to 1.5% and 1000, if E>2. In addition to mobility, the average melt fraction in the cube was dependent on the settings of the largest allowed sphere V_{max}, increasing if the latter was set higher.

Regardless of the unrealistic spherical shape of melt lenses in the experiment, this simplification does not significantly affect the output, as the shape is not a parameter in the power law equation, that describes the distribution of the batch volumes.

Presented computer model suggests, that stepwise merger of the melt batches and discontinuous melt extraction can lead to the power law batch size distributions and to the fractality in the partially molten rocks. The value of the power law exponent can be used to evaluate the melt accumulation efficiency in the rock and consequently, efficiency of the melt extraction.

6.2 Conversion of dimensions

As demonstrated by Bons et al. (2004), numerical models can be effectively used to simulate partial melt processes. In order to interpret migmatite formation, one should compare the results of the numerical model with the observations in migmatites. However, although melt segregation and accumulation can be easily modelled three-dimensionally on the computer, the results cannot be directly compared to one-dimensional data set of leucosome thicknesses measured in the drill cores, as well as with the two-dimensional analogue experiment. Following presents mathematical derivation of formulas, that enable to calculate the exponents for the power law distributions of one-dimensional and two-dimensional data, resulting from the different cross-sections through the three-dimensional power law distribution. As well, derived formulas can be used to estimate the volume and cross-cut area distributions for one-dimensional thickness distributions of the objects.

The derivation of the dimension recalculation formulas is based on probabilities of hitting a leucosome with the certain thickness or cross-cut area by a randomly selected

point on a line or surface, respectively (Soesoo et al., 2004 b; J. Kalda, pers. comm., 2005). These probabilities are assumed to be equal in both situations, as both one-dimensional and two-dimensional leucosome size distributions obey the power law. The cross-cut area will be then expressed via leucosome thickness and the resulting distribution exponents will be compared.

If the cumulative number of leucosomes as the function of thickness is

$$N_1 = f_1(h) = A * h^{-\alpha_1} \quad , \tag{1}$$

where A is a constant, h is the thickness and α_1 is the distribution exponent of 1D data, the number of leucosomes with thicknesses in the range [h, h+dh] can be expressed as

$$dN_1([h, h+dh]) = f_1'(h) * dh \qquad \rightarrow \qquad dN_1([h, h+dh]) = A * \alpha_1 * h^{-\alpha_1 - 1} * dh \tag{2}$$

Along the line, the probability of hitting a leucosome with the certain size depends on the leucosome thickness and on the number of leucosomes of that size:

$$dp_1 = h * dN_1 = h * A * \alpha_1 * h^{-\alpha_1 - 1} * dh \quad ,$$

simplifying the expression by replacing constants A and α_1 with A', the result is

$$dp_1 = A' * h^{-\alpha} * dh \tag{3}$$

Next, the same operations will be carried out on two-dimensional data.

The cumulative number of leucosomes as the function of cross-cut area is

$$N_2 = f_2(S) = B * S^{-\alpha_2} \quad ,$$

where α_2 is the distribution exponent of leucosome cross-cut areas.

Leucosome length l is assumed to be a function of thickness like

$$l = X * h^{\beta} \quad , \tag{4}$$

where X is constant and β is the distribution exponent. β=1, when the relation between thickness and length of leucosomes is linear, i.e. the aspect ratio is independent of the leucosome size (cross-cut area).

The area of leucosome would be then

$$S = C * l * h = C * X * h^{\beta} * h = C' * h^{\beta + 1} \quad , \tag{5}$$

where constants C and X will be substituted with constant C'.

The number of leucosomes with an area in the range [S, S+dS] is

$$dN_2([S, S+dS]) = f_2'(S) * dS \tag{6}$$

The derivation of f_2(S) is

$$f'_2(S)=B*\alpha_2*S^{-\alpha_2-1} \quad \rightarrow \quad f'_2(S)=B'*S^{-\alpha_2-1} \ , \tag{7}$$

where constants B and α_2 are replaced with constant B'.

Differential of S is expressed as

$$dS=S'*dh=C'*(\beta+1)*h^{\beta}*dh=C''*h^{\beta}*dh \ , \tag{8}$$

where S' is the derivation of (5) and constants C' and (β+1) are replaced with C"

Calculating the number of leucosomes by substituting the equations (7) and (8) into the equation (6), the result is

$$dN_2([S,S+dS])=B'*S^{-\alpha_2-1}*C''*h^{\beta}*dh$$

The probability of hitting a leucosome with the area of S is

$$dp_2=dN_2*S=B'*S^{-\alpha_2-1}*C''*h^{\beta}*S*dh \quad \rightarrow \quad dp_2=B'*S^{-\alpha_2}*C''*h^{\beta}*dh \ ,$$

substituting S with the equation (5) and constants B', C' and C" with constant B" to simplify the expression, the probability would be

$$dp_2=B''*h^{-\alpha_2(\beta+1)+\beta}*dh \tag{9}$$

Assuming that probabilities dp_1 and dp_2 are equal, the exponents in expressions (3) and (9) are related as

$$-\alpha_1=-\alpha_2*(\beta+1)+\beta$$

α_1 is then

$$\alpha_1=\alpha_2*(\beta+1)-\beta \ , \tag{10}$$

and α_2

$$\alpha_2=\frac{\alpha_1+\beta}{\beta+1} \ . \tag{11}$$

In three-dimensional situation, β is doubled, as the batch volume can be expressed by

$$V=S*l=X*h^{\beta+1}*h^{\beta}=X*h^{2\beta+1} \ ,$$

in other aspects, the formula derivation path is analogous to that in the two-dimensional situation. Conversion of the thee-dimensional exponent into other dimensions is then

$$\alpha_3=\frac{\alpha_1+2\beta}{2\beta+1} \tag{12}$$

$$\alpha_1=\alpha_3*(2\beta+1)-2\beta \tag{13}$$

$$\alpha_3 = \frac{\alpha_2 * (\beta + 1) + \beta}{2\beta + 1} \tag{14}$$

$$\alpha_2 = \frac{\alpha_3 * (2\beta + 1) - \beta}{\beta + 1} \tag{15}$$

The results are independent of the leucosome shape. It is evident from equation (5), where area S is expressed via thickness h and includes the shape as a constant, not as a parameter.

To apply the conversion formulas to the measured data, some special cases should be examined first. For example, the exponent of the batch volume distribution D=0.67 as the indicator of effective accumulation is converted into D=0 in the one-dimensional case on the ground of (13) and into D=0.5 in the two-dimensional case according to (15). Three-dimensional exponent D=1 as the boundary between the mass accumulation and dispersion is expressed also as D=1 in both one- and two-dimensional cross-sections.

These numbers can be compared with the results of the batch area measurements in the analogue experiment and leucosome thickness distributions in migmatites. The two-dimensional exponent D=0.5 in the analogue model, recalculated to the batch volumes reflects effective accumulation of gas at the initial phase of the experiment, where most of the total gas is contained in few larger batches. Accumulation efficiency decreases gradually with time as progressively more gas is dispersed into preferentially smaller batches at later phases, increasing the exponent to unity and over. Conversion formula can be also used to derive one-dimensional batch size distribution from the batch area distribution, as the direct measuring along a line on the image was barred due to the insufficient number of the objects. The exponent of the batch area distribution D=0.5 approximates to D=0 if the batch thicknesses are measured.

In migmatites, one-dimensional cumulative leucosome thickness distribution exponents with values from D=0.83 to D=1.41 translate into D=0.94 to D=1.14 when respective leucosome volume distributions are calculated. As one can conclude, the accumulation of the melt into large batches is not favoured in measured migmatites.

As the conversion formulas are derived purely on theoretical basis, it would be useful to check their validity also empirically, for instance by using a computer-generated data set. One-dimensional measurements through two-dimensional data consisting of 10 000 objects following the power law with an exponent of 0.67 and distributed randomly in a

square showed, however, deviations from the predicted exponent values. The problem is probably in the oversampling of larger batches, when the generated objects are forced into a space with a finite size and measurements are made over the whole square. The exponent approximated to the predicted value if larger objects were removed from the measurement results. Performed experiments on artificial data were therefore suffering from the finite size scaling effects, which can be avoided by increasing the number of the objects and distribution area, while using a smaller measurement area. This requirement is satisfied e.g. by the measurements in migmatites, where typically the explored outcrop is small compared to migmatized crustal segment. Consequently, regardless the given uncertainties by applying formulas to computer-generated data, there should be no reason to question in the reliability of the dimension conversion formulas.

The conversion formulas include a parameter β, that describes the relationship between the size and aspect ratio of a leucosome. Leucosome width/length ratios as high as 1:150 have been reported (e.g. Barraud et al., 2004), but more extensive statistics about the relationships between aspect ratio and leucosome size is lacking. Therefore, the leucosome width and length relation is assumed to be linear and $\beta=1$, which simplifies the use of the conversion formulas.

6.3 Discussion of analogue experiment results and migmatite data

Although the analysis of analogue experiment results suggested, that no decision can be made about short-term gas segregation processes by studying the development of the batch size distributions and exponents, it is clear that the artificial experimental system can organize itself into a state, where it generates similar fractal structures as observed in migmatites. This state is likely of self-organized critical nature, that can be inferred from the emergence of fractals and the 1/f power spectrum of gas amount fluctuations in the tank, measured and analysed by the author in a former similar experiment (Urtson, 2003), as well as reported by Bons & van Millingen (2001). The small influence of short-term processes on the batch size distribution exponent value can be explained in the light of self-organized criticality. Instead of changing the exponent during the development of the system, the distribution is probably maintained constant over a longer time period, with the exponent being a parameter, which describes the particular self-organized critical state that the system has reached. Therefore, the exponent does not depend on the gas phase

transportation. This conclusion is also supported by the numerical model.

Two experiments with the same materials have been performed formerly by the author (Urtson, unpublished). These experiments showed, however, slightly different exponents. Comparison of the exponents of the first 25 minutes of three analogous experiments show that they vary in the range of d=0.85-0.9, d=0.65-0.86 and d=0.5-0.67, respectively. The reason for such variation between the experiments is unclear. If it rests upon the rate of the carbon dioxide production, then it should depend on the temperature and yeast activity (i.e. freshness) which, however, were not controlled during the experiment. Moreover, from the point of view of self-organized criticality and as suggests the numerical model, the transport rate through the system is not effective on the distribution exponent. As the system reaches the critical state which is described by the distribution exponent of the occurring event sizes, it can transmit any additional amount of the material without further modifications.

The only factor, effective to the distribution exponent, is the mobility of the material, as proposed by Bons et al. (2004). The stress field caused by the overlying sand pile in the analogue experiment is assumed to be homogeneous and without stress gradients. In this case the buoyancy forces are the main agent of the gas transport in the tank. Even if the temperature may theoretically affect the buoyancy of the gas, possible temperature differences are too small to cause remarkable effects. If the different exponents in three analogous experiments are indeed caused by the different mobility, it should be related to some other parameter of the experiment set-up. The role of mechanical properties of sand, e.g. packing density should be considered.

Besides the re-calculated batch volume distribution exponent of 0.67, that implies good accumulation, the average gas fraction of approximately 2% in the tank, similar to the average melt fraction in the numerical model is notable.

Compared to the high accumulation efficiency in the analogue experiment, high exponent values in migmatites reflect poorer accumulation. Also, the melt fraction in migmatites is an order of magnitude higher than the gas fraction in the analogue experiment. According to the numerical model, the melt fraction in the system is dependent on the mobility of the melt and on the critical volume of the batch, that would escape the system. This should be consistent with the behaviour of the gas, which mobility must be relatively higher due to its lower viscosity than the mobility of silicate melt in migmatites, resulting in the lower melt fraction and distribution exponent in the analogue

experiment. The escape of the material is controlled by buoyancy forces in the analogue experiment and the same occurs most probably also in migmatites. The buoyancy is more efficient when the density contrast between melt and solid phase is sharper. However, the phase density contrast is obviously greater in the analogue experiment, which allows the gas to escape more easily, with simultaneous decrease in the size of the batch that could stay in the system. Thus, comparing the analogue experiment and migmatites, the better accumulation and lower gas fraction in the former can be explained by the higher mobility of the gas, which is caused by its low viscosity, and lower critical batch size due to sharper contrasts between gas and solid (sand+water) phase densities. Relatively high viscosity of the melt and small differences in melt and solid phase densities may result in the high melt fraction but poor accumulation of melt in migmatites, characterized by high values of leucosome width distribution exponents.

Inferring the melt batch volumes from the power law distributions with particular exponents, possible melt extraction efficiency has been obtained on theoretical basis. In the case of high accumulation efficiency (D=0.67), as much as 94% of melt can be extracted without leaving traces in the form of leucosomes, whereas melt extraction reduces to zero, if D=1 (Soesoo et al., 2004 b; Bons et al., 2004). According to this, all measured migmatites with the exponents close to one should not have experienced melt loss. At this stage, the comparison of modelling results and estimations of melt production on the ground of geochemical data should be invoked. Unfortunately, such data as the reference are not yet available for measured migmatites.

If the efficiency of the melt accumulation and extraction from the rock is closely related to the melt mobility, which in turn is controlled by the melt viscosity, as well as by tectonic stresses, a couple of more questions arise. First, melting of the crust under different conditions will probably result in varying distributions, which can be characteristic to particular combinations of temperature, pressure and rock composition. And secondly, if the distribution exponent, measured in a migmatite, is the function of temperature and tectonic regime, how will it behave if temperature decreases and stresses die out? If it re-organizes into a state of lower melt mobility with different leucosome distribution, the evidence of former melt accumulation and extraction processes will possibly be overprinted. This can be the reason, why all measured migmatites display exponents close to one at the last stage of melting prior to final freezing.

7. CONCLUSIONS

The fractality of migmatite structures and processes of crustal melting, melt segregation, accumulation and transport, involved in migmatite formation, were studied using analogue and numerical methods. The results of measurements in migmatites were combined with data from an analogue experiment and a computer simulation, in order to investigate the dynamics of magma processes.

Leucosome thicknesses were measured along line traverses in six drill cores from the Estonian crystalline basement and in two outcrops- Masku in the Turku area, southern Finland and Montemor-o-Novo in central Portugal. The leucosome thickness distributions followed the power law in most measured migmatites, with exponents varying in the range of D=0.83-1.41. To support the interpretation of the development of such scale invariant structure in migmatites, an experiment was carried out in a flat glass tank, using sand and carbon dioxide as analogues of solid and melt phases in the partial melting processes of the crust. The stepwise transport and accumulation of the gas resulted in the power law batch area distribution with the exponent around 0.5.

The recalculations of leucosome thickness and gas batch area distributions to the corresponding volume distributions suggest effective gas accumulation in the analogue experiment, whereas the melt accumulation into larger leucosomes is not favoured in migmatites. As suggests the numerical model, the mobility can be the dominant factor in driving the melt and gas accumulation. The lower exponent in the analogue experiment is explained by higher mobility of the gas due to its lower viscosity, relatively high viscosity of silicate melts in migmatites may result in low mobility and poor accumulation. An order of magnitude higher melt fraction in migmatites than the average gas fraction in the analogue experiment suggests the low buoyancy of melt due to its small density contrast with solid matrix, increasing the critical size of a melt batch, that could leave the system by buoyancy forces and thus, increasing also the melt fraction inside the migmatite. The behaviour of melt and resulting leucosome size distributions under different temperature and stress conditions should be considered.

If the poor accumulation, inferred from the leucosome thickness distribution exponents reflects also poor melt extraction efficiency, the melt has been not extracted from measured migmatites or more plausible, the evidence of former processes is overprinted by the last stage melting processes in the cooling crustal segment with probably lower melt mobility.

The general emergence of the scale invariance in both natural and artificial systems implies the incorporation of an universal mechanism- the self-organized criticality.

ACKNOWLEDGEMENTS

Author is thankful to Jaan Kalda from the Institute of Cybernetics at Tallinn University of Technology for his valuable help with mathematical problems. The research was financially supported by the target funding programme No. 0332652s04, the fieldwork and building of the experiment unit were funded by Estonian Science Foundation grants No. 4615 and No. 5301, respectively.

REFERENCES

Armienti, P., Tarquini, S. 2002. Power law olivine crystal size distributions in lithospheric mantle xenoliths. *Lithos* 65, 273-285.

Bak, P., Tang, C., Wiesenfeld, K. 1987. Self- organized criticality: an explanation of 1/*f* noise. *Physical Review Letters* 59, 4, 381-384.

Bak, P., Tang, C., Wiesenfeld, K. 1988. Self-organized criticality. *Physical Review A* 38, 364-374.

Bak, P. 1997. How nature works: the science of self-organized criticality. *Oxford University Press.*

Barraud, J., Gardien, V., Allemand, P., Grandjean, P. 2004. Analogue models of melt-flow networks in folding migmatites. *Journal of Structural Geology* 26, 307-324.

Blower, J. D., Keating, J. P., Mader, H. M., Phillips, J. C. 2001. Inferring volcanic degassing processes from vesicle size distributions. *Geophysical research letters* 28, 347-350.

Bonnet, E., Bour, O., Odling, N. E., Davy, P., Main, I., Cowie, P., Berkowitz, B. 2001. Scaling of fracture systems in geological media. *Reviews of Geophysics* 39, 3/ August, 347-383.

Bons, P. D., van Millingen, B. P. 2001. New experiment to model self-organized critical transport and accumulation of melt and hydrocarbons from their source rock. *Geology* 29, 10, 919-922.

Bons, P.D., Arnold, J., Elburg, M.A., Kalda, J., Soesoo, A., van Milligen, B.P. 2004. Melt extraction and accumulation from partially molten rocks. *Lithos* 78, 25-42.

Clark, M. B., Brantley,S. L., Fisher, D. M. 1995. Power-law vein-thickness distributions and positive feedback in vein growth. *Geology* 23, 975-978.

Engelbrecht, J., Uus, A. 1993. Mittelineaarne dünaamika ja kaos. *Tallinn.*

Johannes, W., Ehlers, C., Kriegsman, L. M., Mengel, K. 2003. The link between migmatites and S-type granites in the Turku area, southern Finland. *Lithos* 68, 69-90.

Kivisilla, J., Niin, M., Koppelmaa, H., 1999. Catalogue of chemical analyses of major elements in the rocks of the crystalline basement of Estonia. *Estonian Geological Survey.*

Knesel, K. M., Davidson, J. P 1999. Sr isotope systematics during melt generation by

intrusion of basalt into continental crust. *Contributions to Mineralogy and Petrology* 136, 285-295.

Koistinen, T., Klein, V., Koppelmaa, H., Korsman, K., Lahtinen, R., Nironen, M., Puura, V., Saltikova, T., Tikhomirov, S. & Yanovskiy, A. 1996. Paleoproterozoic orogenic belt in the surroundings of the Gulf of Finland. In: *Explanation to the Map of Precambrian basement of the Gulf of Finland and surrounding area 1:1 mill.* (Koistinen, T., ed.). *Geological Survey of Finland, Special Paper*, 21, 21-57.

Kriegsman, L. M. 2001. Partial melting, partial melt extraction and partial back reaction in anatectic migmatites. *Lithos* 56, 75–96.

Laporte, D., Watson, E. B. 1995. Experimental and theoretical constraints on melt distribution in crustal sources: The effect of crystalline anisotropy on melt interconnectivity. *Chemical Geology* 124, 161-184.

Maaløe, S. 1992. Melting and diffusion processes in closed-system migmatization. *Journal of Metamorphic Geology* 10, 503-516.

Malamud, B. D., Turcotte, D.L. 1999. How many plumes are there? *Earth and Planetary Science Letters* 174*,* 113-124.

Mandelbrot, B. 1967. How long is the coast of Britain? Statistical self-similarity and fractional dimension. *Science* 156, 636-638.

Marchildon, N., Brown, M. 2003. Spatial distribution of melt-bearing structures in anatectic rocks from Southern Brittany, France: implications for melt transfer at grain- to orogen-scale. *Tectonophysics* 364, 215-235.

Mengel, K., Richter, M., Johannes, W. 2001. Leucosome-forming small-scale geochemical processes in the metapelitic migmatites of the Turku area, Finland. *Lithos* 56, 47-73.

Moores, E. M., Fairbridge, R. W. (eds.) 1994. Encyclopedia of European and Asian regional geology. *Chapman&Hall,* 611-618.

Pereira, M. F., Silva, J. B. 2002. The geometry and kinematics of enclaves in sheared migmatites from the Evora Massif, Ossa-Morena Zone (Portugal). *Geogaceta* 31, 199-202.

Petersell, V., Levchenkov, O. 1994. On the geological structure of the crystalline basement of the southern slope of Baltic shield. *TÜ Toimetised* 972, 16-39.

Petford, N., Cruden, A. R., McCaffrey, K. J. W., Vigneresse, J.-L. 2000. Granite magma formation, transport and emplacement in the Earth's crust. *Nature* 408, 7, 669-673.

Puura, V., Vaher, R., Klein, V., Koppelmaa, H., Niin, M., Vanamb, V., Kirs, J. 1983. Кристаллический фундамент Эстоний. *Nauka.*

Puura, V., Hints, R., Huhma, H., Klein, V., Konsa, M., Kuldkepp, R., Mäntari, I., Soesoo, A. 2004. Svecofennian metamorphic zones in the basement of Estonia. *Proceedings of Estonian Academy of Sciences, Geology,* Special Issue 53 (3), 190-209.

Roberts, S., Sanderson, D., Gumiel, P. 1999. Fractal analysis and percolation properties of veins. In *Fractures, Fluid Flow and Mineralisation* (McCaffrey, K., Lonegran, L. , Wilkinson, J., eds.). *Geological Society, London, Special Publications*, 155, 7-16.

Rothman, D. H., Grotzinger, J. P., Flemings, P. 1994. Scaling in turbidite deposition. *Journal of Sedimentary Research* A64*,* 59-67.

Sawyer, E. W. 2001. Melt segregation in the continental crust: distribution and movement of melt in anatectic rocks. *Journal of metamorphic Geology* 19, 291-309.

Silva, J. B., Pereira, M. F. 2004. Transcurrent continental tectonics model for the Ossa-Morena Zone Neoproterozoic Paleozoic evolution, SW Iberian Massif, Portugal. *The International Journal of Earth Sciences, Geologische Rundschau* 93, 886-896.

Soesoo, A., Puura, V., Kirs, J., Petersell, V., Niin, M., All, T. 2004 a. Outlines of the Precambrian basement of Estonia. *Proceedings of Estonian Academy of Sciences, Geology,* Special Issue 53 (3), 149-164.

Soesoo, A., Kalda, J., Bons, P.D., Urtson, K., Kalm, V. 2004 b. Fractality in geology: a possible use of fractals in the studies of partial melting processes. *Proceedings of Estonian Academy of Sciences, Geology* 53, 13-27.

Turcotte, D. L. 1992. Fractals and chaos in geology and geophysics. *Cambridge University Press.*

Urtson, K. 2003. Analoogmodelleerimise võimalustest maakoore osalise ülessulamise uurimisel. Bachelor's thesis. *Institute of Geology, University of Tartu,* Tartu.

Vigneresse, J. L., Barbey, P., Cuney, M. 1996. Rheological transitions during partial melting and crystallization with application to felsic magma segregation and transfer. *Journal of Petrology* 37, 6, 1579-1600.

Vigneresse, J. L., Burg, J.P. 2000. Continuous vs. discontinuous melt segregation in migmatites: insights from a cellular automaton model. *Terra Nova* 12, 188-192.

Walte, N. P., Bons, P. D., Passchier, C. W., Koehn, D. 2003. Disequilibrium melt distribution during static recrystallization. *Geology* 31, 11, 1009-1012.